ABSTRACT

Title of Document: MODELING SOIL RESPONSE TO INTENSE HEATING FROM TUNNEL FIRES

Xianxu Hu, Master of Science, 2006

Directed By: Professor André Marshall, Department of Fire Protection Engineering; and
Professor Deborah Goodings, Department of Civil and Environmental Engineering

This study investigates the response of saturated soils to intense heating from tunnel fires by numerical simulation. A general purpose commercial CFD code, FLUENT and a special porous media code, TOUGH2, are used. The conservation equations for porous media in each program are discussed and the numerical models are established. Two-dimensional simulations for the saturated coarse sand and the saturated fine sand are conducted and the results are compared with experimental data. It was found that models for capillary effects and relative permeability are required to describe the experimentally observed behavior. Without considering them, FLUENT predicts an inconsistent dry-out vapor zone in the soil column. TOUGH2 which includes these models gives the same two-zone structure observed in experiments, namely a liquid zone on the top and a two-phase zone at the bottom. The TOUGH2 results provide insight into the experimentally observed transient phenomena and agree well with experimentally observed trends.

MODELING SOIL RESPONSE TO INTENSE HEATING FROM TUNNEL FIRES

By

Xianxu Hu

Thesis submitted to the Faculty of the Graduate School of the
University of Maryland, College Park, in partial fulfillment
of the requirements for the degree of
Master of Science
2006

Advisory Committee:
Professor André Marshall, Chair
Professor Deborah Goodings
Professor Arnaud Trouvé

Acknowledgements

This work has been funded by the National Science Foundation under Grant No. 0331332.

First of all, I would like to thank my advisors, Prof. Marshall and Prof. Goodings, for their wonderful guidance, support and interesting discussions. Their hard work and support have inspired me to try my best to conduct this research.

I would also like to thank all of the professors in the Department of Fire Protection Engineering and colleagues in the FETS Lab for giving me a good environment to study and conduct this research.

Special thanks go to all of my friends for their encouragement and assistance during my M.S. study.

Finally but not the least, I want to give my sincere thanks to my husband, my parents in law and my parents, who have supported me all through this work, for their understanding and encouragement.

Table of Contents

List of Tables

List of Figures

Nomenclature

A	Area, m^2
C_e	Evaporation or condensation area coefficient
c_p	Specific enthalpy, kJ/kg-K
d_p	Solid particle diameter, m
D	Diameter of the soil column, m
E	Evaporation or condensation coefficient in the phase change rate model
E_b	The total emissive power of a black body, W/m^2
F	Force in the momentum equation, N; View factor in the heat flux calculation
$\vec{g}$	Gravity acceleration, m/s^2
H	Height, m
h	Specific enthalpy in TOUGH2 approach, kJ/kg
h_e	Interfacial heat transfer coefficient, kW/m^2-K
h_{fg}	Latent heat, kJ/kg
h_q	Sensible enthalpy for phase q in FLUENT approach, kJ/kg
J	Radiosity, W/m^2
k	Thermal conductivity of the phase, W/m-K
k_{eff}	Effective thermal conductivity of the fluid mixture, W/m-K
k_t	Turbulent thermal conductivity, W/m-K

k_{rp}	Relative permeability of the phase p
k_{rl}	Relative permeability of the liquid phase
k_{rv}	Relative permeability of the vapor phase
K	Intrinsic permeability of the porous medium, m^2
L	Width of the porous medium layer, m
m	Mass, kg
$\dot{m}_{l\to v}$	Net phase change rate per unit volume from the liquid phase to the vapor phase, kg/m^3-s
$\dot{m}_{qp}$	Mass rate per unit volume transferred from the phase q to the phase p , kg/m^3-s
$\dot{m}_{pq}$	Mass rate per unit volume transferred from the phase p to the phase q , kg/m^3-s
M	Molecular weight of water, kg/kmol
n	The direction normal to a surface in equations (2-2) and (2-3) Numbers of the fluid phases in other equations.
p	Pressure, Pa
p_c	Capillary pressure, Pa
q	Rate of heat transfer, W
$\dot{q}''$	Heat flux, kW/m^2
r	Radius, m
R	Universal gas constant, R = 8.314 kJ/kmol-K
S	Liquid saturation

S_E	Energy source term, kW/m^3
S_p	The degree of saturation for the phase p
S_{lr}	The residual saturation of the liquid phase
S_{ls}	The maximum saturation of the liquid phase
S_{gr}	The residual saturation of the gas phase
T	Temperature, K
t	Time, s
u	Specific internal energy, kJ/kg
v_{fg}	Change of the specific volume during evaporation, m^3/kg
$\vec{v}$	Darcy velocity, m/s
$\vec{v}_n$	Darcy velocity normal to a surface, m/s
$\vec{V}$	Physical velocity, m/s
$\vec{V}_{dr,p}$	Drift velocity of the phase p , m/s
V	Volume, m^3
x	Coordinate
y	Coordinate
	Moisture content in Eq. (2-47)
z	Coordinate

Greek letters

α	Volume fraction of a fluid phase to the total void space
φ	Porosity of the porous medium

ε	Emissivity
λ	Effective thermal conductivity of the porous medium, W/m-K
ρ	Density, kg/m^3
μ	Dynamic viscosity, N-s/m^2

Subcsripts

g	Gas
l	Water liquid
m	Mixture of the fluid phases
p	Phase index
q	Phase index
ref	Reference
s	Solid matrix
sat	Saturation
v	Water vapor
∞	Ambient

Chapter 1: Introduction

The fire safety in tunnels has become an international issue following catastrophic tunnel fires worldwide. As a result, a significant increase in research and investigation of tunnel fires has resulted in a much better understanding of tunnel fire safety issues. Principle issues include problems related to fluid dynamics such as smoke management and problems related to structure such as the response of the concrete tunnel lining to intense heating from fires. But little attention is given for the relationship between tunnel fires and the soil surrounding a tunnel. This chapter introduces the motivation of this project, examines the previous work done which is related to this topic, and presents the objectives of this thesis.

1.1 Motivation

Accident fires in tunnels can cause disastrous consequences including loss of life, property and potentially severe damage of the tunnel structure. Table 1 lists some cases of severe tunnel fires. Except the Howard St. Tunnel fire (Baltimore USA, 2001), the other cases all involve injury, vehicle damage and serious structural damage of the tunnel lining.

The spalling of the concrete tunnel lining subjected to intense heating was the key factor for the structure damage in these fires. However, it is also possible that the extreme heat and prolonged duration typically involved in a tunnel fire may also change the behavior of the soil surrounding a tunnel, which may adversely affect the

stability of the tunnel lining due to increased pore water pressure in the soil and possible soil migration. As shown in Figure 1, when fire occurs in a tunnel, the water inside the surrounding soil could vaporize causing excess pore water pressure to generate in the soil. The increased pore water pressure reduces the effective stress carried out by the soil matrix and therefore the shear resistance of the soil matrix. Consequently, voids could be formed due to possible soil migration. Voids along the soil-tunnel lining interface and the reduced shear stress of the soil matrix could lead to excessive deformation of the tunnel lining.

Table 1. Selected tunnel fires [1 - 3]

Year	Tunnel	Duration of fire	Consequences		
			People	Vehicles	Structure
1979	Nihonzaka (Japan)	159 hrs	7 dead 1 injured	127 trucks 46 cars	Serious damage
1996	Channel tunnel (England-France)	2.5 hrs $T_{max}\approx700\ ^{o}C$	30 injured	10 trucks	Severe damage
1999	Mont Blanc (France-Italy)	53 hrs $T_{max}\approx1000\ ^{o}C$	39 dead	23 trucks 10 cars 1 motor 2 fire engines	Serious damage
1999	Tauern (Austria)	15 hrs	12 dead 49 injured	14 trucks 26 cars	Serious damage
2001	St. Gotthard (Switzerland)	48 hrs	11 dead	13 trucks 4 vans 6 cars	Serious damage
2001	Howard St. Tunnel (USA)	48 hrs $T_{max}\approx800^{o}C$	Damage to telecoms cables and major business interruption		
2005	Fréjus (France – Italy)	6 hrs	2 dead 21 injured	4 trucks 3 fire engines	Serious damage

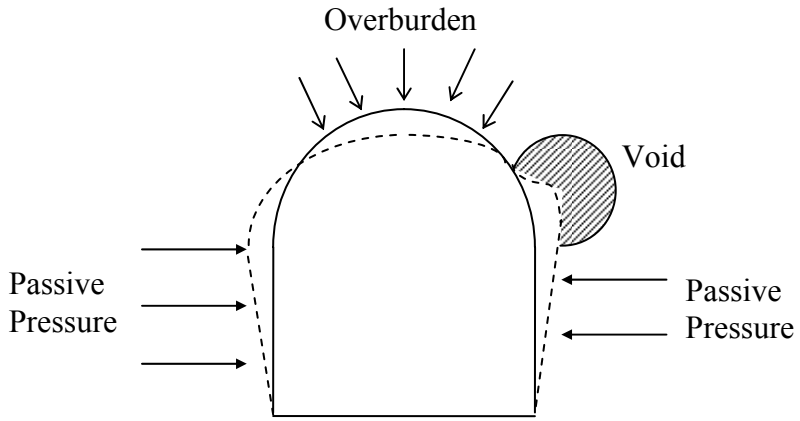

Figure 1. Description of lining load indicating possible soil-lining interaction

The problem involving concrete spalling under sever tunnel fires has been studied by many researchers, but little attention has been given to explore the possible effects of the surrounding soil on the stability of the tunnel lining under severe tunnel fires. To predict the transient soil behavior under severe fires, Yong [3] at the University of Maryland conducted an experimental study in a 1.5 m high soil column heated at the bottom with a heat flux of about 33 kW/m^2. In his experiments, the centerline temperatures and pore water pressures were measured for different types of water-saturated soils and unsaturated soils. He found at the onset of boiling, a liquid zone exists above an underlying two-phase layer, which is at saturation temperature ($\approx$100 ^oC). The leading front of the two-phase zone, named the saturation temperature front propagates upward as time increases. This propagation speed in the coarse sand is about 2 times that of the fine sand. Furthermore, the pore water pressure inside the soil increases greatly in finer-grain soils, which is nearly 400% of the effective stress carried out by the soil matrix before fires.

This research provides some interesting insight into possible transport behavior in soils surrounding a fired tunnel. However, the geometry difference between the soil column and the actual tunnel geometry limits the utility of the results to a qualitative discussion. For a real tunnel, the soil response surrounding a fired tunnel in terms of thermal transport, soil densification, and dissipation of water and water vapor will be influenced by the three-dimensional nature of the configuration, and a one-dimensional configuration may concentrate and even exaggerate soil response in many instances. Furthermore, the soil cover depth represented in these experiments, 1.5 m, is also small for a tunnel. However, the limited resources available for this research did not allow for field tests with real tunnel fires. Even in the laboratory, it is challenging to prepare large amounts of soils for large scale tests. Therefore, numerical modeling is used to predict the transient soil behavior under such extreme conditions. Consequently, the purpose of this project is to establish a numerical model and verify it with experimental data. This validated model could then be used to evaluate the influence of the surrounding soil on the tunnel lining stability under severe tunnel fires in actual tunnel configurations.

1.2 Literature Review

Soil is a natural porous medium. The problem involving soil response under severe tunnel fires is a problem with coupled thermo-hydro-mechanical (THM) phenomena. By further neglecting the mechanical effects such as the deformation of the soil matrix, it is basically a problem involving multiphase flow and heat and mass transfer in porous media, which has been extensively studied in a number of scientific

and engineering disciplines, including geothermal reservoirs, heat pipe technology, nuclear waste disposal, buried electrical cable conduits, drying processes, oil reservoir engineering and groundwater contamination by non-aqueous phase liquids.

In the following literature review, previous research is divided into four groups: natural convection in porous media, boiling in porous media, mechanical response of soils to temperature variations, and coupled thermo-hydro-mechanical (THM) analyses.

1.2.1 Natural convection in porous media

When saturated porous media or unsaturated porous media are heated, the change of the medium temperature may cause a change in the fluid density, so that natural convection may be expected to develop within the porous medium.

Bau [4, 5] examined experimental studies and theoretical analysis on the natural convection structure under steady state conditions in a vertical circular cylinder, which was filled with water saturated porous media and heated from bottom and cooled from top. The critical Rayleigh number for determining the onset of convection was presented. It was found that natural convection occurs in porous media with higher permeability and that the non-axisymmetric single cell convection is the preferred mode for a slender circular cylinder, for which an 'S-shaped' curve can be observed from the centerline temperature profile. While this study was limited to steady state and non-boiling conditions, this research gave good insight into the natural convection phenomena in porous media.

1.2.2 Boiling in porous media

The high heat flux associated with tunnel fires not only induce natural convection, but can also cause boiling in porous media. To investigate the boiling process inside a homogeneous porous medium, a significant number of experimental, theoretical and numerical studies have been conducted.

In the area of experimental studies in short sand or glass bead columns heated at the bottom and cooled on the top, Bau [4, 6] measured the temperature distribution for boiling process in porous media under steady state. He found that boiling can occur before or after natural convection. Under boiling but without dry-out, a quasi-isothermal two-phase zone (liquid and vapor) adjacent to the heating surface exists in the porous medium. The height of the two-phase zone increases with the increase of the heat flux. Above the two-phase zone, a liquid zone is observed either conduction dominated if no natural convection happens or convection dominated if natural convection exists. Udell [7, 8] also carried out steady state experiments in a short sand column for top heated and horizontally heated cases. With dry-out, he found a stable three-zone structure which included (from top to bottom) a superheated vapor zone, a liquid and vapor two-phase zone and a liquid zone. The vapor zone is conduction dominated. The two-phase convection zone is nearly isothermal and exhibits a countercurrent flow of liquid to the heated end and vapor to the cooled end. The compressed liquid zone is also conduction dominated. The length of the two-phase zone decreases with increasing heat flux.

In the area of theoretical analysis, Bau [4, 6] presented a steady state 1-D model to predict the height of the two-phase zone, the dry-out heat flux, and a necessary

condition for the formation of a two-phase zone, by neglecting capillary effects and assuming an isothermal two-phase zone with countercurrent flow of liquid and vapor. In terms of the liquid-layer Rayleigh number at the onset of boiling, the necessary condition for the formation of a two-phase zone was found to be $Ra_b = \frac{gK\beta_l(T_{sat} - T_0)H}{\nu_l(\lambda/\rho_l c_{p,l})} \geq 0.3$ for the case of water assuming $T_{sat} - T_0 = 100K$.

When $Ra_b < 0.3$, a vapor layer is expected near the heated surface. Considering the capillary effects, Udell [7] also evaluated the length of the two-phase zone theoretically together with his experiments for the top heated and bottom cooled case. The model predicts a decreasing two-phase zone length with increasing heat flux, which agrees well with the experimental data. Moreover, he found both vapor and liquid within the two-phase zone should be superheated from the analysis of thermodynamic equilibrium between phases. Continuing this analysis, Udell [8] gave a steady state 1-D model to predict the heat and mass transfer within the two-phase zone by assuming an isothermal two-phase zone. A critical dry-out heat flux model was also given. Considering the top heated case, it was found that the countercurrent flow in the two-phase zone must result from the capillary effects. In addition, the two-phase zone length is longer for basally heated systems and shorter if heated from above. When basally heated, the two-phase zone may be infinitely long for low heat fluxes.

Numerical solutions are most prevalent among the previously described porous media research because of the difficulties with controlling, instrumenting and observing transport behavior in experiments. By neglecting capillary effects and

considering the pressure-enthalpy diagram for pure water, Faust [9] and Roberts [10] conducted numerical simulation of fluid flow and energy transport in porous hydrothermal systems. Using the so-called separate flow model (SFM) but also neglecting capillary effects, Ramesh [11] outlined a numerical algorithm for problems involving boiling and natural convection in a saturated porous medium with constant heat flux heated at the bottom. This algorithm solves equations in the liquid and two-phase regions and can continuously track the interface between them by using a moving boundary approach. Finite difference control volume methods were used to discretize these equations and test results demonstrated the ability of this algorithm. To reduce the number of differential equations brought by the SFM method and avoid tracking explicitly the moving interface between the liquid and two-phase region, Wang [12, 13] developed a single-component multiphase mixture model and simulated the problem of boiling with thermal convection in a porous layer heated from below by applying this model. In his model, phase change was described through the thermodynamic relationships and capillary effects were represented by the Leverett capillary pressure function. Good agreement is achieved between the numerical results and the published previous experiments. Furthermore, Wang [14] extended this single-component multiphase model to general multi-component multiphase model. Instead of using the thermodynamic relationship to describe the phase change inside porous media, Shi [15, 16] conducted numerical modeling using a phase change rate model to study boiling heat transfer in porous layers with and without the presence of chimneys. Different from the above studies which use enthalpy in the energy equation, Benard [17] presented a new mathematical model

where the energy equation relied on an entropy balance adapted to the case of a rigid porous medium. The equilibrium thermodynamic state of water (liquid, vapor or two-phase) was determined by calculating the Gibbs potential with the pressure and temperature condition of the fluid.

Other researchers have also investigated problems involving boiling in unsaturated porous media. Daurelle [18] modeled transient processes of superheated steam drying in unsaturated porous media by a finite element method and obtained the phase change rate with time evolution from the results. Olivella [19] discussed capillary effects related to water evaporation and vapor transport in unsaturated soils by using CODE_BRIGHT. In addition, a model was presented to calculate the intrinsic permeability for clays that changed its structure when wetting-drying occurred.

The previous research has made significant progress for problems involving boiling in porous media, while little has been focused on transient behavior at conditions relevant to soil surrounding a tunnel involved in a severe fire. Furthermore, few results about the excess pore water pressure and the vapor front propagation in the soil are reported.

1.2.3 Mechanical response of soils to temperature variations

From the view of material mechanics, Campanella [20] tested the volume changes and pore pressure changes due to temperature variations from 40^{o}F to 140^{o}F in saturated clays. They found that under drained conditions and constant effective stress, increased temperature results in permanent consolidation of the specimen.

Under un-drained conditions and constant total stress, temperature rise can cause significant excess pore water pressures to generate inside the saturated clays. They also defined a temperature-induced pore pressure parameter, F, and tests on different saturated clays showed that F had a range of only 0.0075 $^{o}F^{-1}$ to 0.010 $^{o}F^{-1}$.

However, this study is limited to steady state and uniform temperature conditions below 140^{o}F, and no boiling phenomena occur.

1.2.4 Coupled thermo-hydro-mechanical (THM) analyses

Except the phenomena of heat and mass transfer, the mechanical properties of the solid matrix may also change due to the temperature change and pressure change inside the porous medium. Rutqvist [21] developed a methodology to link TOUGH2 and FLAC3D to conduct coupled thermal-hydrologic-mechanical (THM) analysis of multiphase fluid flow, heat transfer, and deformation in fractured porous rock. Gens [22] carried out THM analysis on the interacting phenomena associated with the simultaneous heating and hydration of an engineered bentonite barrier placed in a drift excavated in granite by using CODE_BRIGHT. Rutqvist [23] presented coupled THM processes at the Yucca Mountain Drift Scale Test (DST) with four different numerical models (TOUGH-FLAC, CODE_BRIGHT, CASTEM and FLAC) conducted by four teams. A generally good agreement is achieved between simulations and field measurements.

The approach that also considers the change of the mechanical properties of the solid matrix into our problem is ideal in concept, but will make the problem more complex. Hence, as an initial step to understand the soil response under tunnel fires,

the change of soil mechanical properties is neglected and only the phenomena with boiling in rigid porous media is studied in this thesis.

1.3 Codes for Solving Porous Medium Problems

Codes for solving porous medium problems can be grouped into three categories: individual codes developed by the researchers for specific applications, general commercial CFD software and specialized porous media software.

For the numerical modeling discussed previously, most researchers used their individual codes for specific applications. For the purpose of research individually, developed codes provide the preferred route, but this approach involves a multi-year effort. Due to the time and fund limitation of this project along with its specific focus, it is not suitable for us to develop the codes by ourselves.

Use of commercial CFD software can potentially reduce or eliminate the code development time, but such software which can meet all of the features of porous media problem including boiling and capillary effects is not available. Some CFD software such as FLUENT [24] has general capabilities for solving porous media problems, but users need to add the boiling features into the software by themselves and also no capillary effects are available. In addition, like other commercial software, e.g. STARCD, porous media in FLUENT are modeled by the addition of a momentum sink term to the standard fluid flow equations. As a result, this generated momentum equation is somewhat different with the common momentum equation for porous media which is typically reduced to Darcy's law or an extended form of

Darcy's law. Therefore, it is uncertain whether FLUENT is a suitable solver for this project.

There are limited well-developed codes especially for solving porous media problems, including CODE_BRIGHT [25] and TOUGH2 [26]. CODE_BRIGHT is a general-purpose finite element program developed by the Department of Geotechnical Engineering and Geosciences at the Universitat Politècnica de Catalunya (UPC) in Spain for the analysis of coupled thermo-hydro-mechanical (THM) phenomena in geological media. TOUGH2 is a public-domain program developed by DOE in USA. It adopts the integral finite difference method and can model non-isothermal flows of multi-component, multiphase fluids in one, two, and three-dimensional porous and fractured media. The chief applications for which TOUGH2 is designed are in geothermal reservoir engineering, nuclear waste disposal, environmental assessment and remediation, and unsaturated and saturated zone hydrology. A review of this software suggests that it is suitable for this project. But its source code is written in FORTRAN and therefore it doesn't have a friendly computer-human interface for users to define the problem and deal with the results. In addition, unlike the commercial CFD software, only limited technical supports can be provided. To help users rapidly develop models and view results, PetraSim [27] is developed by Thunderhead Engineering. It is an interactive pre-processor and post-processor for TOUGH2, T2VOC, TMVOC, TOUGHREACT, TOUGH-Fx/HYDRATE, and TETRAD, which model non-isothermal flows of multi-component, multiphase fluids in porous and fractured media. It also embeds the core calculation program of TOUGH2 so that users can also run TOUGH2 in Petrasim. In

this study, Petrasim is used to set up the problem and view results while TOUGH2 is used to solve the governing equations.

1.4 Objectives

The objective of this research is to determine which models are capable of simulating the soil response to intense heating and to evaluate their performance through comparisons with the previous soil column experiments [3]. Based on the literature and code review provided in the previous section, FLUENT and TOUGH2 have been identified as candidate simulation tools for this study. FLUENT, a widely available commercial CFD code, was chosen to see how a multi-purpose CFD code would perform in this porous media application. Alternatively, TOUGH2 was chosen because it has been proven to solve a wide variety of porous media problems. The detailed objectives and overall approach for this study are summarized in Figure 2 and discussed below:

1) Formulate the numerical problem for saturated soils according to the previous soil column experiments [3].
2) Identify and select the appropriate models in FLUENT and TOUGH2 to simulate the saturated soil response to intense heating through comparisons with the previous soil column experiments [3].
3) Analyze excess pore water pressures and the vapor front propagation speed from the results.

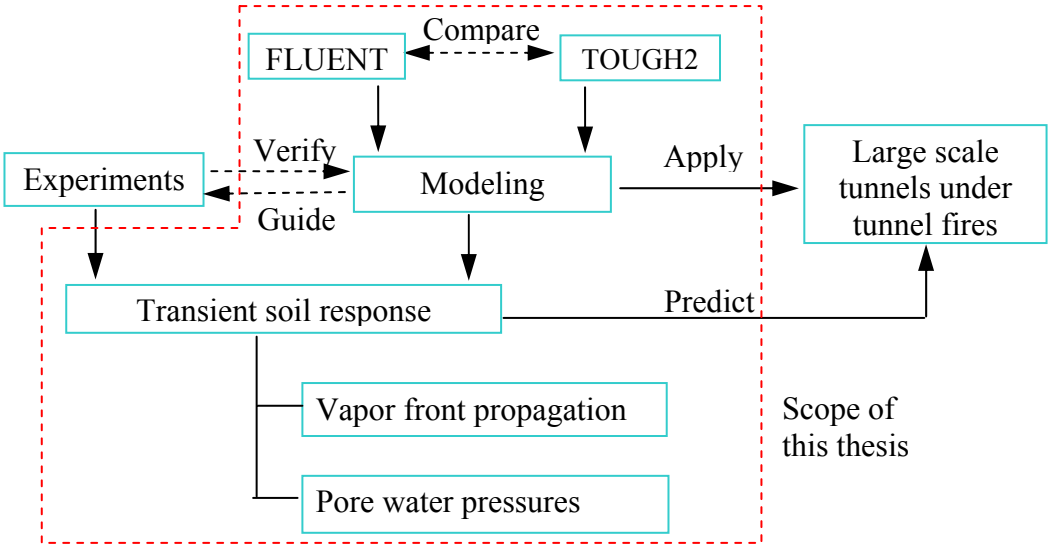

Figure 2. Summary of objectives and approach used in this study

Chapter 2: Approach

Transport processes in porous media can be described at the microscopic (pore-scale) or macroscopic (Representative Elementary Volume) level. For the problem in this project, describing the porous medium at the pore scale level is too complex and unnecessary. By using the continuum approach, this chapter describes the geometric considerations and conservation equations used.

2.1 Continuum Approach

The continuum approach considers the fluid as a continuum and treats the real medium as a fictitious one within which any physical fluid property is averaged over a well chosen Representative Elementary Volume (REV). The length scale of the REV should be much larger than the pore scale, but considerably smaller than the length scale of the macroscopic flow domain to lead to some meaningful averaged quantities reflecting microscopic transport phenomena [28].

To fulfill the macroscopic description of transport behavior in porous media, new macroscopic material properties and flow properties are introduced in the enumerated list that follows.

1) Porosity, φ (m^3/m^3), characterizes the presence of void spaces in a porous medium.

2) Saturation, S_p (m^3/m^3), expresses the volume ratio of fluid phase p such as the liquid phase to void spaces when two or more immiscible fluid phases share the same available void spaces.

3) Intrinsic permeability, K (m^2), takes into account the macroscopic influence of the solid matrix from the standpoint of resistance to the flow. The more permeable a porous medium is, the less it will resist an imposed flow.

4) Relative permeability, k_{rp} (m^2/m^2), relates the permeability of fluid phase p to the intrinsic permeability K which is defined for a single-phase flow. Many investigators conclude from experiments that when several immiscible fluids flow simultaneously through a porous medium, each fluid establishes its own tortuous paths, which in fact form a network of very stable channels.

5) Darcy velocity, $\vec{v}$ (m/s), is a fictitious velocity which assumes that flow occurs across the entire REV. The relationship between the Darcy velocity and the physical velocity, $\vec{V}$ (m/s), is $\vec{v} = \varphi\vec{V}$ for a single phase flow or $\vec{v}_q = \varphi\alpha_q\vec{V}_q$ for a phase q in a multiphase flow, where, α_q (m^3/m^3) is the volume ratio of the phase q to the void spaces.

Furthermore, to describe the macroscopic multiphase flow behavior in problems involving boiling in porous media, the phase change rate model or thermodynamic relationships, Darcy's law and a model describing the possible capillary effects are also required.

2.2 Geometric Considerations

Young [3] carried out experimental studies on transient soil response to extreme heat from tunnel fires. In his experiments, a steel tube with a height of 1.5 m and a diameter of 0.10 m is used to contain soils, as shown in Figure 3. The tube is insulated at sides and heated by a powerful infrared radiant heater from the bottom. The top of the soil column opens to the ambient and the base and sides are watertight. Temperatures and pressures are measured at different heights along the column centerline. For the experiments of saturated soil, a water column of about 10 cm is maintained on the top of the soil column to make sure the soil is always saturated. The aspect ratio of the soil column is $H_1/D = 12$ and the aspect ratio of the water layer is $H_2/D = 1$ with $D = 0.10$ m in the soil column experiments.

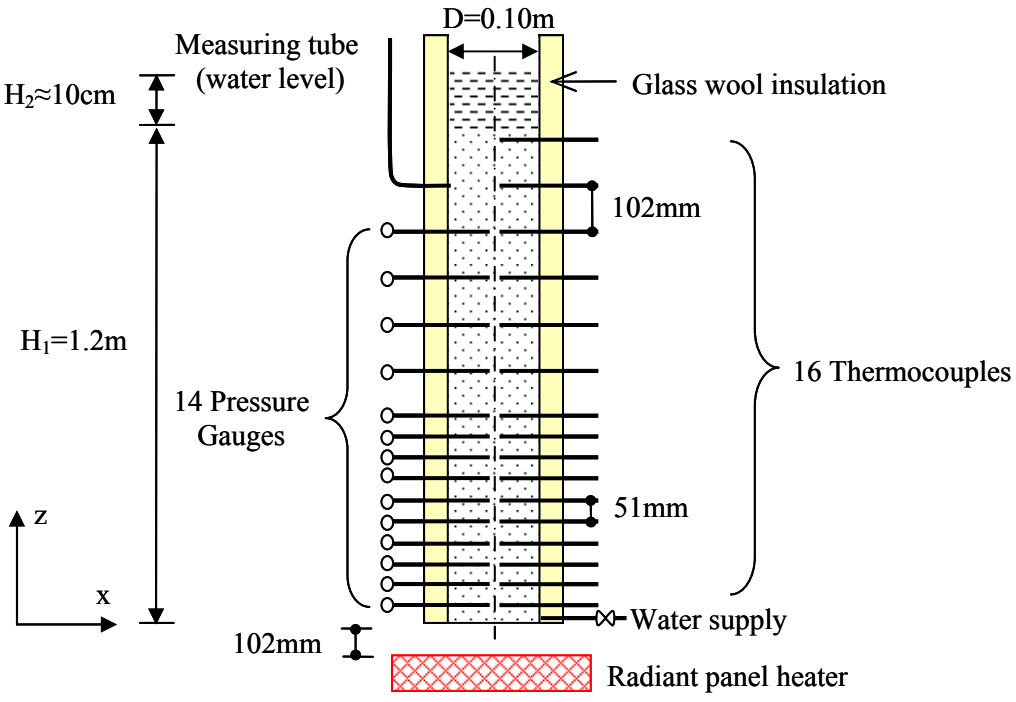

Figure 3. Experimental geometry

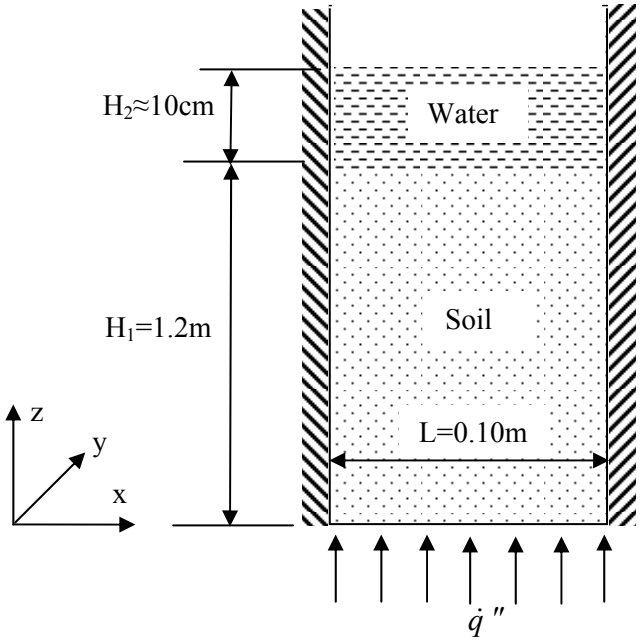

Figure 4. Modeling geometry

In this computational study, it was prohibitive to use expensive 3-D simulations of the experimental configuration to explore the large parameter space of interest which included different CFD codes and models. Limitations of computer power required an approximate approach where the experimental configuration is represented by the 2-D geometry (infinite in y) shown in Figure 4. This approximation is based on the assumption that the insulated experimental cylinder configuration with the large aspect ratio is dominated by transport in the z-direction. It is recognized that the 2-D predictions of convection behavior will be inherently different from those occurring in the cylindrical experimental configuration. However, the details of those convection effects are assumed to play a secondary role to the dominant capillary and phase change transport processes. The quality of the

agreement between simulations and experiments can be used as a metric to evaluate this assumption.

The time savings aimed by using a 2-D simulation are profound. For example, 2-D simulations in FLUENT take approximately 2 weeks on a standard PC; whereas, 3-D simulations take 2 months. Similarly, TOUGH2 takes several hours to model a 2-D case and more than 2 weeks to model a 3-D case. Furthermore, 3-D simulations of the experimental configuration were attempted but they provided unphysical solutions and more time is needed to solve this problem.

The boundary and the initial conditions of the 2-D model are:

$$z = H_1 + H_2, \quad p = p_\infty = 1 \text{ atm}, \tag{2- 1}$$

$$x = \pm\frac{L}{2}, \quad \frac{\partial T}{\partial n} = 0, \quad \vec{v}_n = 0, \tag{2- 2}$$

$$z = 0, \quad -k\frac{\partial T}{\partial n} = \dot{q}'', \quad \vec{v}_n = 0, \tag{2- 3}$$

$$t = 0, \quad T = T_\infty, \quad \vec{v} = 0. \tag{2- 4}$$

2.3 Conservation Equations

As reviewed in §1.3, for the treatment of porous media in the commercial CFD software which has general capabilities for solving porous media problems, a momentum sink term is added to the standard fluid flow equations. Therefore, the mass conservation equation, momentum conservation equation and energy conservation equation are all solved in the problem. While for the treatment of porous media in codes specifically for porous media, only the mass and energy conservation equations are solved, with the Darcy velocity given by Darcy's law.

In the following discussion, the complete set of conservation equations and reduced set of conservation equations are discussed, together with the supplementary equations to close the problem in each set.

2.3.1 Complete set of equations

To model this problem with a commercial CFD software, the mixture model is selected. Taking FLUENT as an example, the mixture model [24] solves the continuity equation for the mixture, the momentum equation for the mixture, the energy equation for the mixture, and the volume fraction equation for the secondary phases, as well as algebraic expressions for the relative velocities if the phases are moving at different velocities.

For general multiphase flow, the governing equations of the mixture model can be written as:

Continuity equation

$$\frac{\partial}{\partial t}\left(\rho_m\right)+\nabla\cdot\left(\rho_m\vec{V}_m\right)=0, \tag{2- 5}$$

Volume fraction equation for the secondary phase *p*

$$\frac{\partial}{\partial t}\left(\alpha_p\rho_p\right)+\nabla\cdot\left(\alpha_p\rho_p\vec{V}_m\right)=-\nabla\cdot\left(\alpha_p\rho_p\vec{V}_{dr,p}\right)+\sum_{q=1}^{n}\left(\dot{m}_{qp}-\dot{m}_{pq}\right), \tag{2- 6}$$

Momentum equation

$$\begin{aligned}\frac{\partial}{\partial t}\left(\rho_m\vec{V}_m\right)+\nabla\cdot\left(\rho_m\vec{V}_m\vec{V}_m\right)=&-\nabla p+\nabla\cdot\left[\mu_m\left(\nabla\vec{V}_m+\nabla\vec{V}_m{}^T\right)\right]\\&+\rho_m\vec{g}+\vec{F}+\nabla\cdot\left(\sum_{q=1}^{n}\alpha_q\rho_q\vec{V}_{dr,q}\vec{V}_{dr,q}\right),\end{aligned} \tag{2- 7}$$

Energy equation

$$\frac{\partial}{\partial t}\sum_{q=1}^{n}\left(\alpha_q \rho_q E_q\right)+\nabla\cdot\sum_{q=1}^{n}\left(\alpha_q \vec{V}_q\left(\rho_q E_q + p\right)\right)=\nabla\cdot\left(k_{eff}\nabla T\right)+S_E, \tag{2- 8}$$

where

$$\rho_m = \sum_{q=1}^{n}\alpha_q \rho_q , \tag{2- 9}$$

$$\vec{V}_m = \frac{\sum_{q=1}^{n}\alpha_q \rho_q \vec{V}_q}{\rho_m}, \tag{2- 10}$$

$$\vec{V}_{dr,q} = \vec{V}_q - \vec{V}_m , \tag{2- 11}$$

$$\mu_m = \sum_{q=1}^{n}\alpha_q \mu_q , \tag{2- 12}$$

$$k_{eff} = \sum_{q=1}^{n}\alpha_q \left(k_q + k_t\right). \tag{2- 13}$$

For an incompressible phase,

$$E_q = h_q = \int_{T_{ref}}^{T} c_{p,q}\, dT . \tag{2- 14}$$

For a compressible phase,

$$E_q = h_q - \frac{p}{\rho_q} + \frac{v_q^{\,2}}{2} = \int_{T_{ref}}^{T} c_{p,q}\, dT - \frac{p}{\rho_q} + \frac{v_q^{\,2}}{2} . \tag{2- 15}$$

The treatment for porous media in FLUENT is basically to introduce the porosity into each term of each equation, add a momentum sink term into the general momentum equation and include the solid phase into the transient term and the

conduction flux term in the energy equation. By assuming: 1) the porous medium is isotropic; 2) the solid matrix is rigid; 3) at any point of the continuous medium, the three phases are locally at thermal equilibrium ($T_s = T_l = T_v = T$), the governing equations of the mixture model for multiphase flow in porous media can be written as below:

Continuity equation

$$\frac{\partial}{\partial t}(\varphi\rho_m) + \nabla\cdot(\varphi\rho_m\vec{V}_m) = 0\,, \tag{2- 16}$$

Volume fraction equation for the secondary phase *p*

$$\frac{\partial}{\partial t}(\varphi\alpha_p\rho_p) + \nabla\cdot(\varphi\alpha_p\rho_p\vec{V}_m) = -\nabla\cdot(\varphi\alpha_p\rho_p\vec{V}_{dr,p}) + \varphi\sum_{q=1}^{n}(\dot{m}_{qp} - \dot{m}_{pq}), \tag{2- 17}$$

Momentum equation

$$\begin{aligned}&\frac{\partial}{\partial t}(\varphi\rho_m\vec{V}_m) + \nabla\cdot(\varphi\rho_m\vec{V}_m\vec{V}_m) = -\varphi\nabla p + \nabla\cdot\left[\varphi\mu_m\left(\nabla\vec{V}_m + \nabla\vec{V}_m{}^T\right)\right]\\ &+ \varphi\rho_m\vec{g} + \varphi\vec{F} + \nabla\cdot\left(\varphi\sum_{q=1}^{n}\alpha_q\rho_q\vec{V}_{dr,q}\vec{V}_{dr,q}\right) - \left(\frac{\mu}{K} + \frac{C_2\rho_m}{2}\left|\vec{V}_m\right|\right)\vec{V}_m\end{aligned}, \tag{2- 18}$$

Energy equation

$$\begin{aligned}&\frac{\partial}{\partial t}\left(\sum_{q=1}^{n}(\varphi\alpha_q\rho_q E_q) + (1-\varphi)\rho_s E_s\right) + \nabla\cdot\sum_{q=1}^{n}\left(\varphi\alpha_q\vec{V}_q(\rho_q E_q + p)\right)\\ &= \nabla\cdot\left((\varphi k_{eff} + (1-\varphi)k_s)\nabla T\right) + \varphi S_E\end{aligned}. \tag{2- 19}$$

Since h_q in equations (2-14) and (2-15) is defined as the sensible enthalpy in FLUENT, an energy source term should be applied into the above energy equation (2-19) in order to include the boiling phenomena. This energy source term can be written as:

$$\varphi S_E = -\dot{m}_{l\to v}h_{fg}\,. \tag{2- 20}$$

where, $\dot{m}_{l\to v}$ is the net phase change rate from the water liquid to the water vapor.

To further simplify the solution, the following is neglected:

1) the inertia loss term, $\frac{C_2\rho_m}{2}\left|\vec{V}_m\right|\vec{V}_m$, in the momentum equation, since the flow velocity in this problem is not expected to be high;
2) the velocity difference between fluid phases, since the drift velocity model in FLUENT needs the bubble diameter but it is unknown in this problem.

The governing equations describing this problem (boiling in saturated soils) can be written in the form provided below by limiting the fluid phases to liquid and vapor:

Continuity equation

$$\frac{\partial}{\partial t}\left(\varphi S\rho_l+\varphi(1-S)\rho_v\right)+\nabla\cdot\left(\left(\varphi S\rho_l+\varphi(1-S)\rho_v\right)\vec{V}_m\right)=0\,, \qquad (2\text{-}21)$$

Volume fraction equation for the vapor phase *v*

$$\frac{\partial}{\partial t}\left(\varphi(1-S)\rho_v\right)+\nabla\cdot\left(\varphi(1-S)\rho_v\vec{V}_m\right)=\dot{m}_{l\to v}\,, \qquad (2\text{-}22)$$

Momentum equation

$$\begin{aligned}&\frac{\partial}{\partial t}\left(\left(\varphi S\rho_l+\varphi(1-S)\rho_v\right)\vec{V}_m\right)+\nabla\cdot\left(\left(\varphi S\rho_l+\varphi(1-S)\rho_v\right)\vec{V}_m\vec{V}_m\right)\\&=-\varphi\nabla p+\nabla\cdot\left[\left(\varphi S\mu_l+\varphi(1-S)\mu_v\right)\left(\nabla\vec{V}_m+\nabla\vec{V}_m{}^T\right)\right]\\&+\left(\varphi S\rho_l+\varphi(1-S)\rho_v\right)\vec{g}+\varphi\vec{F}-\frac{\mu}{K}\vec{V}_m\end{aligned}\,, \qquad (2\text{-}23)$$

Energy equation

$$\begin{aligned}&\frac{\partial}{\partial t}\left(\varphi S\rho_l E_l+\varphi(1-S)\rho_v E_v+(1-\varphi)\rho_s E_s\right)\\&+\nabla\cdot\left(\varphi S\vec{V}_m\left(\rho_l E_l+p\right)+\varphi(1-S)\vec{V}_m\left(\rho_v E_v+p\right)\right)\\&=\nabla\cdot\left(\left(\varphi Sk_l+\varphi(1-S)k_v+(1-\varphi)k_s\right)\nabla T\right)-\dot{m}_{l\to v}h_{fg}\end{aligned}\,. \qquad (2\text{-}24)$$

Equations (2-21) to (2-24) provide 4 equations but 10 unknowns (ρ_l, ρ_v, S, $\vec{V}_m$, $\dot{m}_{l\to v}$, p, E_l, E_v, E_s, T). In addition to the Boussinesq assumption for the liquid density, Ideal gas law for the vapor density, and equations (2-14) to (2-15) which can provide 3 equations (1 equation for each phase), an additional supplementary equation or relationship is still required to close this problem.

There are two alternatives to provide this supplementary equation or relationship. One is using the empirical formulas from thermodynamics which relate the thermodynamic properties of pure water and water vapor to the dependent variables - pressure and enthalpy. The other is determining the phase change rate $\dot{m}_{l\to v}$. To simplify the connections between the mathematical model and FLUENT, the phase change rate model is selected to close this problem. This model will be integrated into FLUENT through the User Defined Functions (UDF).

Since there is no universal correlation for the phase change rate in porous media, the expressions of boiling and condensation rate based on the phase change rate developed by Shi [15] are used. They are

$$T \geq T_{sat}, \quad \dot{m}_{l\to v} = \frac{C_e \dfrac{6S(1-\varphi)}{d_p} h_e (T - T_{sat})}{h_{fg}}, \tag{2- 25}$$

$$T < T_{sat}, \quad \dot{m}_{l\to v} = \frac{C_e \dfrac{6(1-S)(1-\varphi)}{d_p} h_e (T - T_{sat})}{h_{fg}}, \tag{2- 26}$$

where

$$h_e = \frac{2E}{2-E}\left(\frac{M}{2\pi R}\right)^{1/2} \frac{{h_{fg}}^2}{{T_{sat}}^{3/2} v_{fg}}. \tag{2- 27}$$

In above equations, C_e is the evaporation or condensation area coefficient, E is the evaporation or condensation coefficient, M is the molecular weight of water, R is the universal gas constant, and v_{fg} is the change of specific volume during evaporation. In the literature written by Shi [15, 16], C_e has a value of 0.02, which was determined through comparison of simulations with available experimental results from the literature. In the book written by Collier [29], the value of E for water is 0.03−0.05.

To summarize, the unknowns and available equations for FLUENT approach are shown in Table 2.

Table 2. Unknowns and available equations for FLUENT approach

Equation description	Unknowns	No. of equations provided
Continuity equation (2-21)	ρ_l, ρ_v, S, $\vec{V}_m$	1
Volume fraction equation for the vapor phase (2-22)	ρ_v, S, $\vec{V}_m$, $\dot{m}_{l\to v}$	1
Momentum equation (2-23)	ρ_l, ρ_v, S, $\vec{V}_m$, p	1
Energy equation (2-24)	ρ_l, ρ_v, S, $\vec{V}_m$, p, E_l, E_v, E_s, T, $\dot{m}_{l\to v}$	1
Definition of E in FLUENT (2-14) to (2-15)	ρ_v, $\vec{V}_m$, p, E_l, E_v, E_s, T	3
Boussinesq assumption	ρ_l, T	1
Ideal gas law	ρ_v, T, p	1
Boiling and condensation model (2-25) to (2-27)	S, T, $\dot{m}_{l\to v}$	1
Total	10 unknowns: ρ_l, ρ_v, S, $\vec{V}_m$, p, E_l, E_v, E_s, T, $\dot{m}_{l\to v}$	10 equations available

2.3.2 Reduced set of equations

From the view of governing equations used especially for porous media, TOUGH2 is selected. TOUGH2 [26] adopts an integral finite difference method and the basic mass and energy balance equations solved by TOUGH2 can be written in the general form

$$\frac{d}{dt}\int_{V_n} M^{\kappa} dV_n = \int_{\Gamma_n} \vec{F}^{\kappa} \cdot \vec{n} dV_n + \int_{V_n} \dot{q}^{\kappa} dV_n \,, \tag{2- 28}$$

where, V_n is an arbitrary sub-domain of the flow system under study which is bounded by the closed surface Γ_n, M represents mass or energy per volume, $\dot{q}$ denotes sinks and sources, $\vec{n}$ is a normal vector on surface element $d\Gamma_n$ pointing inward into V_n, and $\vec{F}$ denotes mass or heat flux, with κ = 1, ..., NK labeling the mass components such as water, air, etc, and κ = NK + 1 labeling the heat component.

In general, the mass accumulation term for mass component κ in a multi-component and multiphase flow system can be written as

$$M^{\kappa} = \varphi \sum_{p} S_p \rho_p X_p^{\kappa} \,, \tag{2- 29}$$

where, X_p^{κ} is the mass fraction of component κ presenting in phase p.

The heat accumulation term in a multiphase system is

$$M^{NK+1} = (1-\varphi)\rho_s c_{p,s} T + \varphi \sum_{p} S_p \rho_p u_p \,, \tag{2- 30}$$

where, u_p is the specific internal energy in phase p.

Neglecting the diffusion between phases, the mass flux is given by

$$\vec{F}^{\kappa} = \sum_{p} X_{p}^{\kappa} \rho_{p} \vec{v}_{p} \ . \tag{2- 31}$$

The heat flux is

$$F^{NK+1} = -\lambda \nabla T + \sum_{p} h_{p} \rho_{p} \vec{v}_{p} \ , \tag{2- 32}$$

where, λ is the effective thermal conductivity of the porous medium.

The Darcy velocity for an individual phase is given by the multiphase version of Darcy's law, which can be written as:

$$\vec{v}_{p} = -\frac{k_{rp} K}{\mu_{p}} \left(\nabla p_{p} - \rho_{p} \vec{g} \right), \tag{2- 33}$$

$$p_{p} = p_{g} + p_{c,p} \, , \tag{2- 34}$$

where, p_{g} is the gas phase pressure and $p_{c,p}$ is the capillary pressure for phase p .

Using Gauss' divergence theorem to equation (2-28), it changes to

$$\frac{\partial M^{\kappa}}{\partial t} = -\nabla \cdot \vec{F}^{\kappa} + \dot{q}^{\kappa} . \tag{2- 35}$$

For saturated soils used in our problem, there is only one flow component (water) and two fluid phases (liquid and vapor). By assuming

1) the porous medium is isotropic,
2) the solid matrix is rigid,
3) at any point of the continuous medium, the three phases are locally at thermal equilibrium ($T_{s} = T_{l} = T_{v} = T$),
4) the mass diffusion between phases can be neglected,

the governing equations with the format given by equation (2-35) can be written as:

Mass equation

$$\frac{\partial}{\partial t}\left(\varphi S\rho_l + \varphi(1-S)\rho_v\right) + \nabla\cdot\left(\rho_l\vec{v}_l + \rho_v\vec{v}_v\right) = 0\,, \tag{2- 36}$$

Energy equation

$$\begin{aligned}&\frac{\partial}{\partial t}\left(\varphi S\rho_l u_l + \varphi(1-S)\rho_v u_v + (1-\varphi)\rho_s c_{p,s}T\right)\\&+\nabla\cdot\left(\rho_l h_l\vec{v}_l + \rho_v h_v\vec{v}_v\right) - \nabla\cdot\left(\lambda\nabla T\right) = 0\end{aligned}\,, \tag{2- 37}$$

Plug $u = h - \frac{p}{\rho}$ into equation (2-40), it can be changed to

$$\begin{aligned}&\frac{\partial}{\partial t}\left(\varphi S\rho_l h_l + \varphi(1-S)\rho_v h_v + (1-\varphi)\rho_s c_{p,s}T\right)\\&-\frac{\partial}{\partial t}\left(\varphi S p_l + \varphi(1-S)p_v\right) + \nabla\cdot\left(\rho_l h_l\vec{v}_l + \rho_v h_v\vec{v}_v\right) - \nabla\cdot\left(\lambda\nabla T\right) = 0\end{aligned}\,, \tag{2- 38}$$

Multiphase version of Darcy's law

$$\vec{v}_l = -\frac{k_{rl}K}{\mu_l}\left(\nabla p_l - \rho_l\vec{g}\right), \tag{2- 39}$$

$$\vec{v}_v = -\frac{k_{rv}K}{\mu_v}\left(\nabla p_v - \rho_v\vec{g}\right), \tag{2- 40}$$

$$p_l = p_v + p_c\,. \tag{2- 41}$$

Equations (2-36) and (2-38) to (2-41) give 5 equations but 15 unknowns which are ρ_l, ρ_v, S, $\vec{v}_l$, $\vec{v}_v$, k_{rl}, k_{rv}, p_l, p_v, p_c, μ_l, μ_v, h_l, h_v, T. To close this problem, additional 9 equations are required. In TOUGH2, these 9 supplementary equations are provided through the relative permeability function which can give 2 equations, the capillary pressure function which can give 1 equation and the water steam table equations which can equivalently give 7 equations.

TOUGH2 provides 8 options for the relative permeability and also 8 options for the capillary pressure. In this study, both the relative permeability and the capillary pressure use the van Genuchten-Mualem model, which is one of the most widely used models.

As introduced in §2.1, in case of two immiscible fluids flowing simultaneously through a porous medium, each fluid establishes its own tortuous paths and a relative permeability for each fluid is defined to describe the extent to which one fluid is hindered by the other fluid or the solid matrix. The van Genuchten-Mualem model of the relative permeability describes this relative hydraulic conductivity of each fluid phase based on the retention data (e.g., the effective degree of liquid saturation ($S^*, \hat{S}$), and the parameter, m, which is related to the shape of the retention curve). It can be described as follows:

$$k_{rl} = \begin{cases} \sqrt{S^*}\left(1-\left(1-\left[S^*\right]^{\frac{1}{m}}\right)^m\right)^2 & if \quad S_l < S_{ls} \\ 1 & if \quad S_l \geq S_{ls} \end{cases}, \tag{2- 42}$$

$$k_{rg} = \begin{cases} 1-k_{rl} & if \quad S_{gr} = 0 \\ \left(1-\hat{S}\right)^2\left(1-\hat{S}^2\right) & if \quad S_{gr} > 0 \end{cases}, \quad 0 \leq k_{rl}, \quad k_{rg} \leq 1, \tag{2- 43}$$

where

$$S^* = \frac{S - S_{lr}}{S_{ls} - S_{lr}}, \tag{2- 44}$$

$$\hat{S} = \frac{S - S_{lr}}{1 - S_{lr} - S_{gr}}. \tag{2- 45}$$

Capillary pressure is induced due to the effect of the interfacial tension between the wetting (i.e., liquid) phase and the non-wetting (i.e., vapor) phase in the soil. The

van Genuchten-Mualem model of the capillary pressure is also based on the effective degree of liquid saturation, S^*, and the parameter, m. It is given by:

$$p_c = -p_0\left(\left[S^*\right]^{-\frac{1}{m}} - 1\right)^{1-m}, \text{ subject to } -p_{\max} \le p_c \le 0, \qquad (2\text{-}46)$$

where, p_0 is a reference pressure and $p_{\max}$ is the negative capillary pressure at which $S \to S_{lr}$.

In above equations, the residual saturation of liquid phase, S_{lr}, the maximum saturation of liquid phase, S_{ls}, the residual saturation of gas phase, S_{gr}, and the parameter, m, can be indirectly determined from the water retention curve in the soil (e.g., the soil-water characteristics curve). Fredlund [30] determined that $S_{lr} \approx 0.1$ for glass beads, $S_{lr} \approx 0.15$ for volcanic sand, $S_{lr} \approx 0.2$ for fine sand and $S_{lr} \approx 0.45$ for Touchet silt loam. In addition, TOUGH2 recommends to always choose a smaller S_{lr} for the capillary pressure as compared to the relative permeability function when using van Genuchten-Mualem mode in order to avoid an unphysical meaning when $S_l \to S_{lr}$. The detail reason for this option can refer to TOUGH2 Userguide [26].

Figure 5 (a) and (b) show an example of the relative permeability profile and capillary pressure profile respectively when $m = 0.457$, $S_{ls} = 1$, $S_{gr} = 0.1$, $1/p_0 = 5.105 \times 10^{-4}$, $p_{\max} = 10^7$, $S_{lr} = 0.15$ for the relative permeability function and $S_{lr} = 0$ for the capillary pressure function.

The steam table equations used in TOUGH2 are based on those equations given by the International Formulation Committee (1967). All water properties such as density, specific enthalpy, viscosity, steam moisture content (or temperature) can be

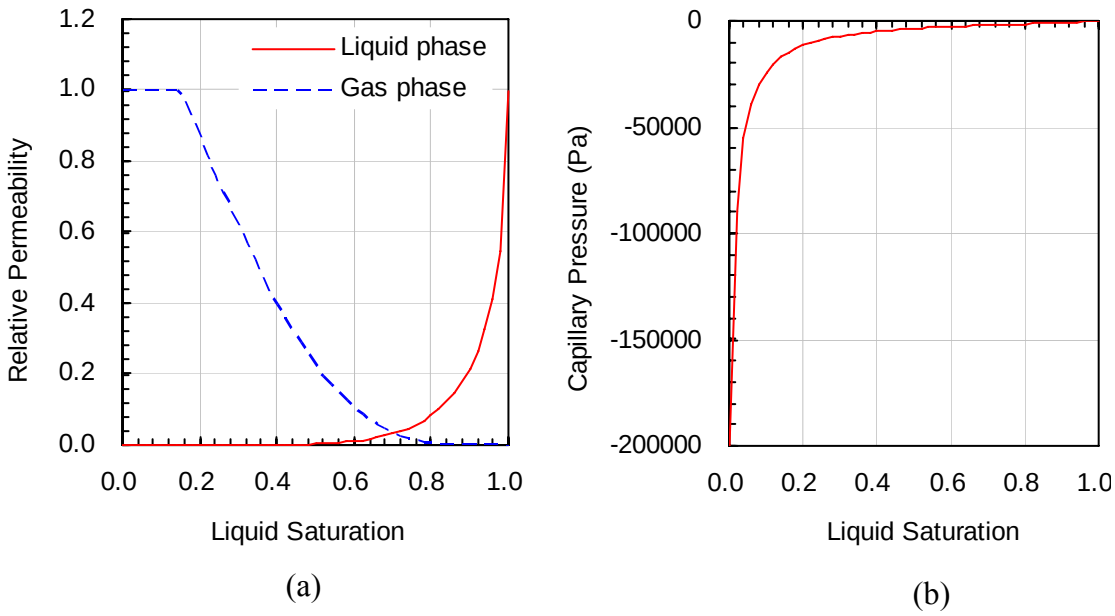

Figure 5. Relative permeability profile and capillary pressure profile
(a) Relative permeability; (b) Capillary pressure

calculated from these steam table equations as a function of the pressure and temperature (or the pressure and the steam moisture content).

Furthermore, since the degree of liquid saturate, S, can be related to the steam moisture content y easily through the following relationship:

$$y = \frac{m_l}{m_l + m_v} = \frac{\rho_l V_l}{\rho_l V_l + \rho_v V_v} = \frac{\rho_l S}{\rho_l S + \rho_v (1 - S)}. \qquad (2\text{-}47)$$

Therefore the steam table equations plus (2-47) are equivalent to provide 7 equations for this problem, from which ρ_l, ρ_v, μ_l, μ_v, h_l, h_v, S (or T) can be solved.

To summarize, the unknowns and available equations for TOUGH2 approach are shown in Table 3.

Table 3. Unknowns and available equations for TOUGH2 approach

Equation description	Unknowns	No. of equations provided
Mass conservation (2-36)	ρ_l, ρ_v, S, $\vec{v}_l$, $\vec{v}_v$	1
Energy conservation (2-38)	ρ_l, ρ_v, S, $\vec{v}_l$, $\vec{v}_v$, p_l, p_v, h_l, h_v, T	1
Darcy's law for the liquid phase (2-39)	ρ_l, $\vec{v}_l$, k_{rl}, p_l, μ_l	1
Darcy's law for the vapor phase (2-40)	ρ_v, $\vec{v}_v$, k_{rv}, p_v, μ_v	1
Definition of capillary pressure (2-41)	p_l, p_v, p_c	1
Relative permeability function for the liquid phase (2-42)	S, k_{rl}	1
Relative permeability function for the vapor phase (2-43)	S, $k_{rv} = k_{rg}$	1
Capillary pressure function (2-46)	S, p_c	1
Steam table equations and (2-47)	ρ_l, ρ_v, S, p_l, p_v, μ_l, μ_v, h_l, h_v, T	7
Total	15 unknowns: ρ_l, ρ_v, S, $\vec{v}_l$, $\vec{v}_v$, k_{rl}, k_{rv}, p_l, p_v, p_c, μ_l, μ_v, h_l, h_v, T	15 equations available

Chapter 3: Results and Analyses

Analyses of 2-D FLUENT and TOUGH2 simulations are provided in this chapter. These analyses focus on centerline temperature profiles, vapor front propagation and the pore water pressure rise in saturated coarse sand and saturated fine sand soil columns. The results are compared with the reference soil column experiments [3].

3.1 Simulation Conditions

3.1.1 Soil properties

Soil properties used in this simulation were selected to match soil characteristics used in Young's reference experiments [3]. Table 4 shows the thermal properties of the soils simulated in this study.

Table 4. Thermal properties of saturated coarse sand and fine sand

Soil Type	Average grain size d_p (μm)	Permeability K (m^2)	Average porosity φ (%)	Effective thermal conductivity λ (W/m-K)
Coarse Sand	1000	2.3×10^{-9}	48%	2.2
Fine Sand	300	7.2×10^{-11}	38%	2.8

3.1.2 Net basal heat flux

In Young's experiments, the control of the net basal heat flux is through the control of the heater temperature which is measured in a thermocouple well near the rough and fused quartz surface of the heater. Young indicated in his thesis [3] that the

soil column irradiation was approximately 33 kW/m^2. However, each experiment has slightly different heater temperatures and greatly different base temperatures measured at the outside surface of the soil column container.

Theoretical boundary conditions are calculated for saturated coarse and fine sand experiments conducted by Young [3]. These boundary conditions will be used in simulations for comparisons with experiments.

The view factor between the heater and the base can be easily calculated by considering the square surface of the heater to be an effective circular plane as shown in Figure 6. The view factors are $F_{12} = 0.6465$ and $F_{21} = 0.0812$, based on

$$F_{21} = \frac{1}{2}\left(B - \left[B^2 - 4\left(\frac{r_1}{r_2}\right)^2 \right]^{\frac{1}{2}} \right), \quad F_{12} = \frac{A_2}{A_1} F_{21}, \tag{3- 1}$$

where, $B = 1 + \dfrac{1 + R_1^{\,2}}{R_2^{\,2}}$, $R_1 = \dfrac{r_1}{H}$, $R_2 = \dfrac{r_2}{H}$.

By further assuming the space is closed by three surfaces as shown in Figure 6, and the room walls are blackbodies, the net heat absorbed by the base and the net heat

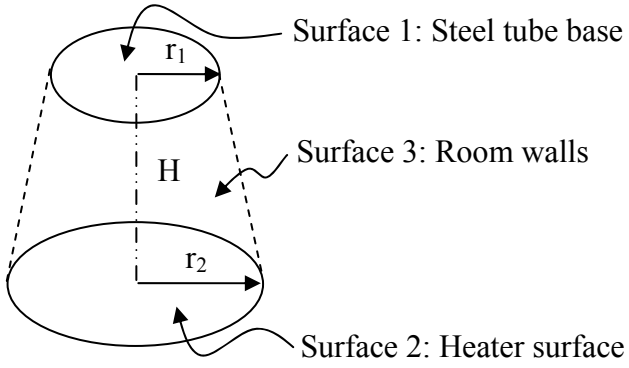

Figure 6. A closed space for calculating the net radiant heat flux

given off by the heater can be written as:

$$q_1 = \frac{E_{b1} - J_1}{\frac{1-\varepsilon_1}{\varepsilon_1 A_1}} = \frac{J_1 - J_2}{\frac{1}{A_1 F_{12}}} + \frac{J_1 - J_3}{\frac{1}{A_1 F_{13}}}, \quad (3\text{- }2)$$

$$q_2 = \frac{E_{b2} - J_2}{\frac{1-\varepsilon_2}{\varepsilon_2 A_2}} = \frac{J_2 - J_1}{\frac{1}{A_2 F_{21}}} + \frac{J_2 - J_3}{\frac{1}{A_2 F_{23}}}, \quad (3\text{- }3)$$

where, $J_3 = E_{b3} = \sigma T_3^4$, $F_{13} = 1 - F_{12}$, $F_{23} = 1 - F_{21}$.

According to the manufacture's data [31], the emissivity of the heater surface (rough and fused quartz) is 0.93. Due to the high temperature used in experiments, the base of the steel tube has already been covered by a layer of soot when the reference experiments used in this thesis were conducted. Therefore, the emissivity of the base is selected to be 0.95 based on the soot emissivity [31].

Figure 7 shows the measured temperatures and calculated net heat flux to the base of the cylinder for the saturated coarse sand experiment conducted on Aug. 13, 2004. The base and heater temperature stabilize at around 310 ^{o}C and 770 ^{o}C respectively. The net basal heat flux is almost a constant after 1 hour. Since the temperature measurement for the heater surface has some delay due to the thermocouple response time, the average value based on the heat flux after 0.5 hour is used in the following simulation, which is about 30 kW/m^2.

Figure 8 shows the measured temperatures and calculated net basal heat flux for the saturated fine sand experiment conducted on July 27, 2004. The base and heater temperature stabilize at around 500 ^{o}C and 710 ^{o}C respectively. Similar as the saturated coarse sand case, the net basal heat flux is also almost a constant after 1

hour. With the same treatment as the saturated coarse sand, the average value based on the heat flux after 0.5 hour is about 11.55 kW/m^2.

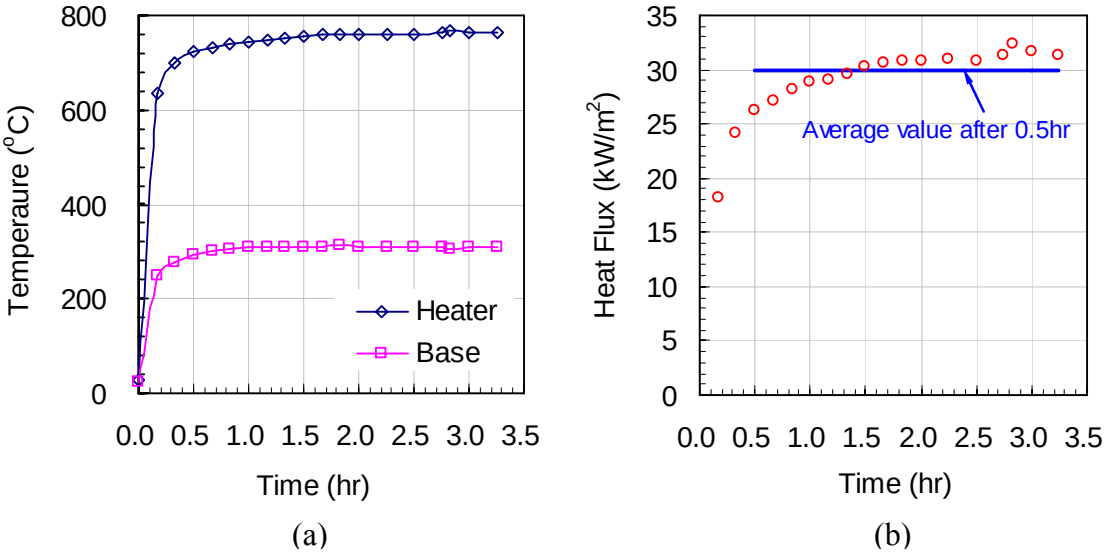

Figure 7. Net basal heat flux for the saturated coarse sand experiment. (a) Heater and base temperature; (b) Calculated net heat flux to the base of the soil column

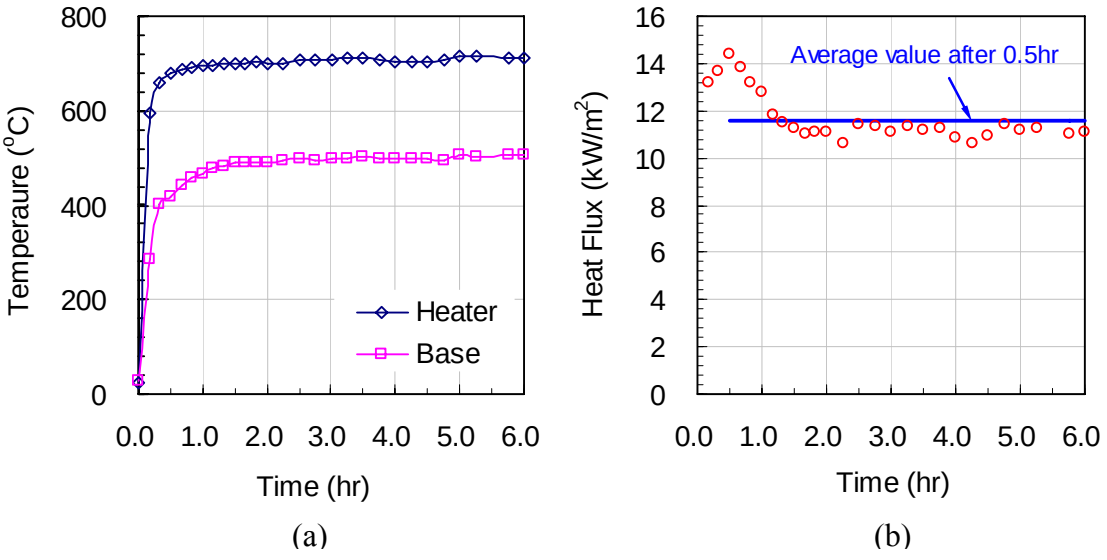

Figure 8. Net basal heat flux for the saturated fine sand experiment. (a) Heater and base temperature; (b) Calculated net heat flux to the base of the soil column

3.2 Preliminary Results

As a preliminary simulation, a 2-D problem with boiling in the saturated coarse sand is modeled in FLUENT with a net basal heat flux of $\dot{q}'' = 33$ kW/m^2. The grid size is 4 mm after optimization and the other parameters are $c_{p,s} = 815$ J/kg-K, $\rho_s = 2650$ kg/m^3, $T_{sat} = 373$ K, $T_\infty = 298$ K, $E = 0.04$, $C_e = 0.02$. Herein, C_e and E use the same values adopted in Shi [15, 16] as discussed in §2.3.1. In addition, a slightly longer column (1.5 m) was used for this preliminary simulation instead of the 1.3 m column used in the experiments. This small discrepancy is not expected to impact qualitative evaluation of the transport behavior or comparisons with experiments.

Figures 9-12 show the development of temperatures and the degree of liquid saturation in the saturated coarse sand soil column with time. Here, the vertical direction is the height of the soil column and the horizontal direction is the width of the soil column. It can be seen that with the increase of heating time, the fluid component changes from single phase (liquid phase) to two phases (liquid phase and vapor phase). When $t = 2$ hours, a three-zone structure appears in the soil column with a vapor zone at the bottom, a liquid zone on the top and a two-phase zone between them. The vapor zone is conduction dominated with linear temperature contours along the horizontal direction. The two-phase zone has upward flow from the sides and downward flow in the middle. In the liquid zone, the top portion of the soil column is conduction dominated but the part near the two-phase zone is convection dominated with small temperature gradients. The shape of the predicted temperature and liquid saturation profiles is consistent to that given by Wang [15],

though Wang's solution is for steady-state and there is no dry-out vapor zone observed.

The leading edge of the vapor front (at the radial boundary) moves upward at a speed of about 0.60 m/hr and the low edge of the vapor front (on the centerline) moves upward at a speed of about 0.40 m/hr. In this study, the vapor front location is defined as the lowest location where the liquid saturation $S = 1$ (e.g., $S = 0.999$ in FLUENT due to accuracy limitations).

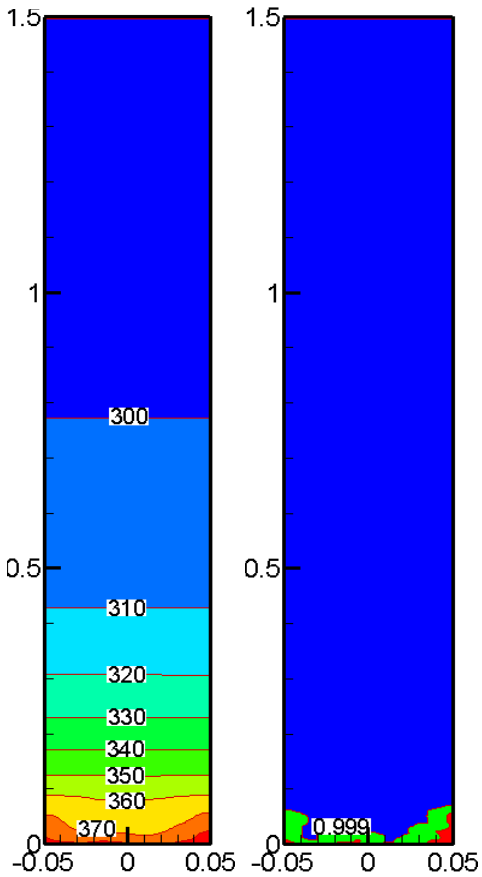

(a) (b)

Figure 9. Fluent simulations of saturated coarse sand soil column experiment at $t = 0.5$ hr. (a) Temperature (K); (b) Liquid saturation.

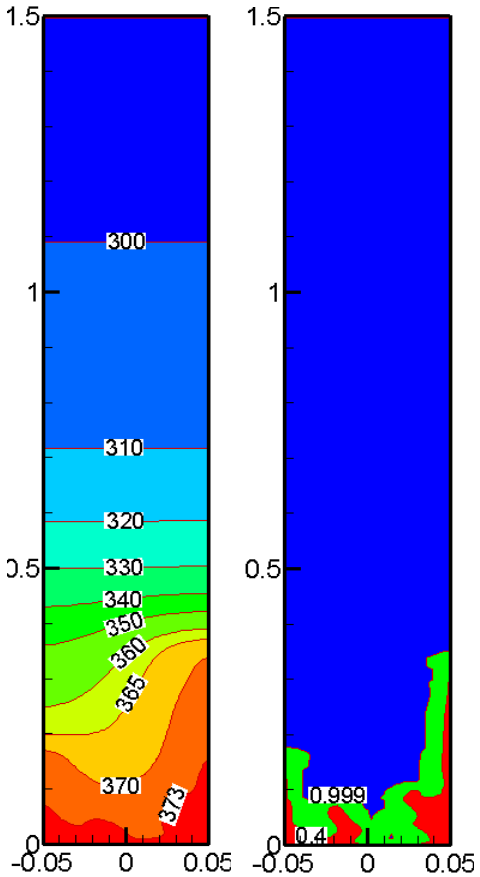

(a) (b)

Figure 10. Fluent simulations of saturated coarse sand soil column experiment at $t = 1.0$ hr. (a) Temperature (K); (b) Liquid saturation.

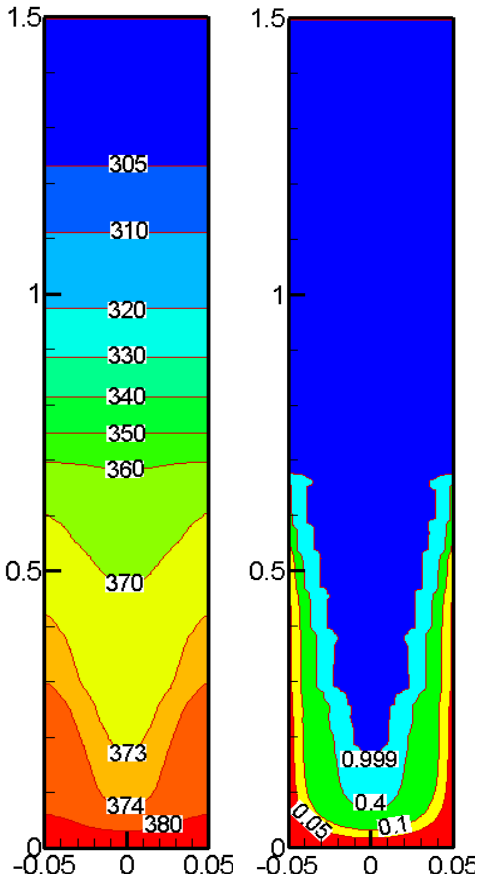

(a) (b)

Figure 11. Fluent simulations of saturated coarse sand soil column experiment at $t = 1.5$ hr. (a) Temperature (K); (b) Liquid saturation.

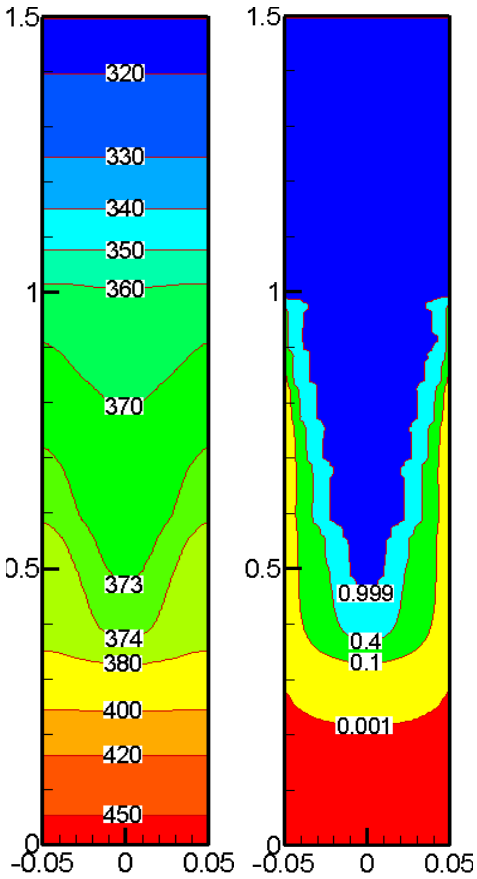

(a) (b)

Figure 12. Fluent simulations of saturated coarse sand soil column experiment at $t = 2.0$ hr. (a) Temperature (K); (b) Liquid saturation.

Figure 13 illustrates the transient development of centerline temperatures in the soil column, which can also indicate the centerline vapor front propagation and the distinct regions developed in the soil column clearly.

The formation of the dry-out vapor zone is possible for boiling problems in porous media. However, in Young's experiments [3], no vapor zone is observed; even

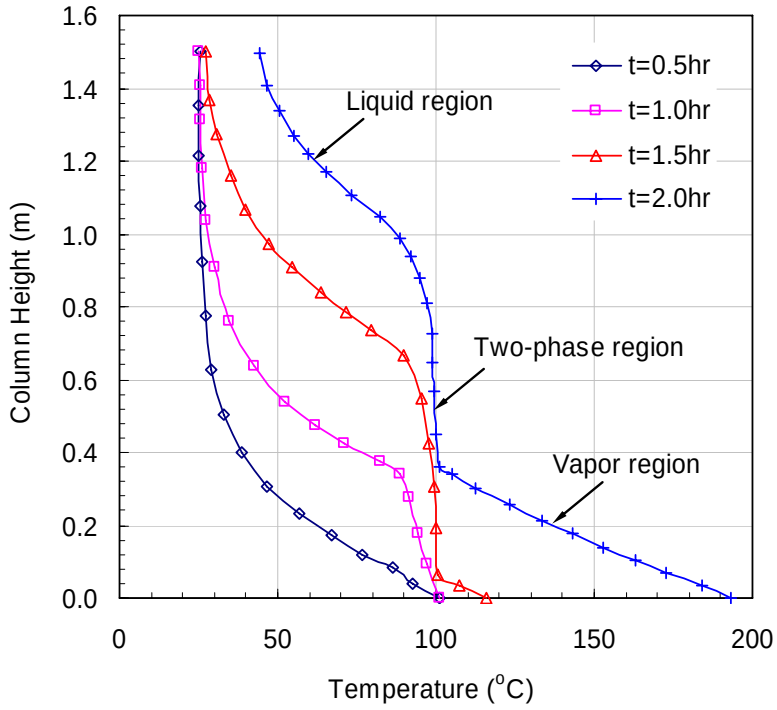

Figure 13. FLUENT simulations of centerline temperatures for the saturated coarse sand soil column experiment

the temperature reading of the lowest thermocouple (0.05 m from the base of the soil column) never exceed the saturation temperature.

The possible reasons for FLUENT to differ from experimental results are:

1) No capillary effects are included in the model. Many studies show that in porous media, the liquid phase and vapor phase in the two-phase zone exist at different pressures due to the effect of the interfacial tension. This pressure difference is equal to the capillary pressure such as given by Eq. (2-46) and can induce liquid from the wetting region to the non-wetting region.

2) No velocity difference between the liquid and vapor phase is considered in the model. As introduced in §2.1, many investigators conclude from

experiments that when several immiscible fluids flow simultaneously through a porous medium, each fluid establishes its own tortuous paths, which in fact form a network of very stable channels. This means the liquid phase and vapor phase will have different permeability to pass through the solid matrix, so that a different velocity exists between the liquid phase and the vapor phase.

3) The constants used in the boiling and condensation models shown in equations (2-25) to (2-27) may not be suitable for this case.

3.3 Refined Results

Because of the limitations of FLUENT described in the previous section, TOUGH2, a code developed specifically for porous media problems, is used which is capable of modeling the capillary effects, the different velocity between the liquid phase and the vapor phase, and uses the steam table equations to describe the phase change instead of empirical boiling and condensation models.

Similar to FLUENT, only 2-D simulations are conducted (see §2.2 for explanation). After optimization, the grid sizes used in the simulation are 2 cm for the height direction and 1.43 cm for the width direction. These grid sizes are sufficiently larger than the pore sizes according to the requirement of the continuum approach. When the porous medium is packed in the loosest way [4], the maximum sphere diameter which can be contained in the pore size is about $\left(\sqrt{3}-1\right)d_p/2 = 0.37\,\text{mm}$ for the coarse sand and $\left(\sqrt{3}-1\right)d_p/2 = 0.11\,\text{mm}$ for the fine sand. Even if the pore sizes

are 2-3 times the maximum sphere diameter, the selected grid sizes are at least an order of magnitude larger than the pore sizes. Additionally, the saturated coarse sand uses a residual saturation of liquid $S_{lr} = 0.15$ in the relative permeability functions and $S_{lr} = 0.10$ in the capillary pressure function (see §2.3.2 for explanation). The saturated fine sand uses a residual saturation of liquid $S_{lr} = 0.20$ in the relative permeability functions and $S_{lr} = 0.15$ in the capillary pressure function (see §2.3.2 for explanation). The other parameters used are $S_{ls} = 1$, $S_{gr} = 0.1$, $c_{p,s} = 815$ J/kg-K and $\rho_s = 2650$ kg/m^3.

3.3.1 Saturated coarse sand

Saturated coarse sand exhibits a complex transport behavior when subjected to intense heating, including water vaporization and condensation, natural convection in the liquid zone, vapor front propagation and pore water pressure rise in the two-phase zone.

Consistent with the reference experiment case [3], TOUGH2 simulations give a two-zone structure with a liquid zone on the top and a two-phase zone at the bottom. Reasonable agreements are also achieved between TOUGH2 simulations and experiments. Figure 14 illustrates the comparison of the centerline temperature development in the saturated coarse sand between simulations and experiments. It can be seen that TOUGH2 simulations qualitatively agree well with the experimental measurements although the leading edge of the two-phase zone is a little lower than that observed in experiments at each time.

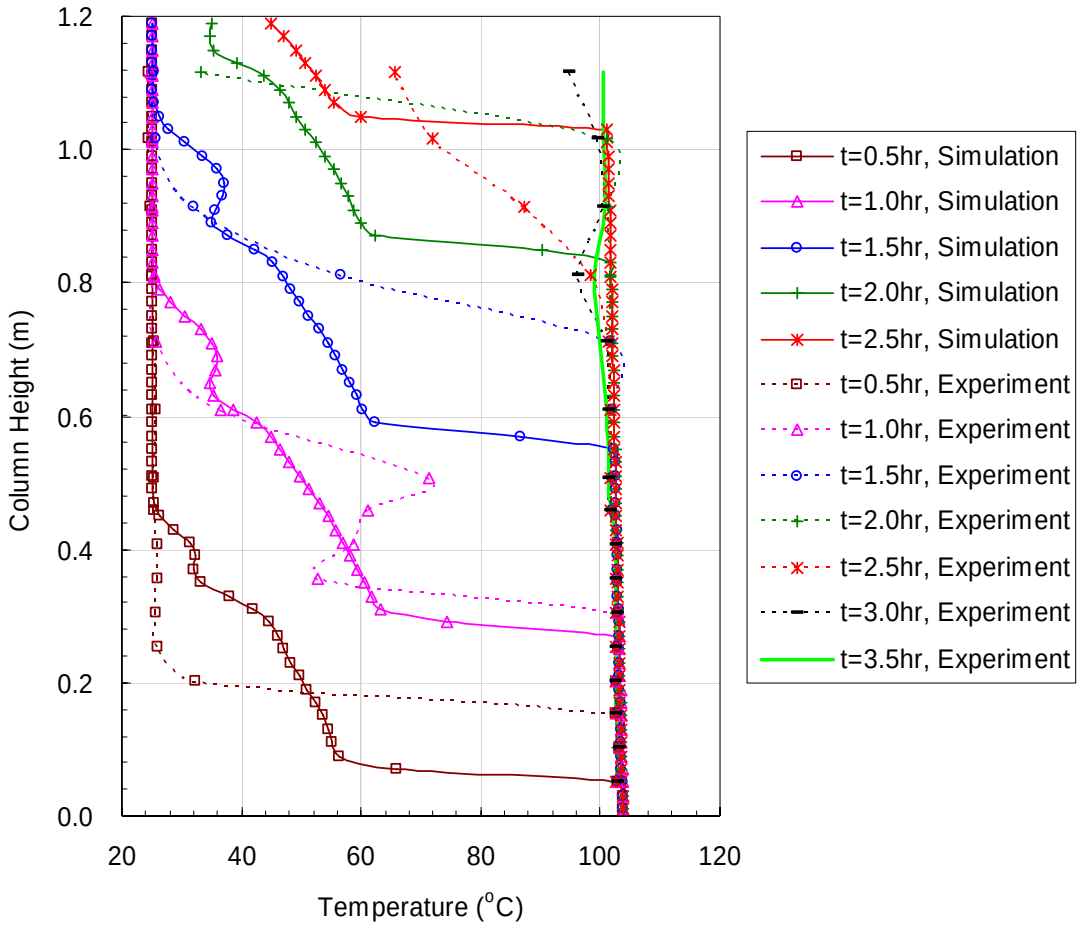

Figure 14. TOUGH2 simulations of centerline temperatures for the saturated coarse sand soil column experiment ($\dot{q}'' = 30$ kW/m^2)

The liquid zone is dominated by natural convection. Shown in Figure 14, an 'S-shaped' curve can be found in each centerline temperature profile before $t = 2$ hours, indicating the occurrence of the single-cell convection in that region at that time [4]. Evaluation of the liquid mass flux profiles (not shown here) proves the existence of the single-cell convection, and also reveals that the convection cell grows during some initial heating period (before 0.5 hour) and maintains a relative stable shape and length after 0.5 hour. During the growing period ($t \leq 0.5$ hour) of the convection cell,

the centerline vapor front doesn't propagate or propagates very slowly, as shown in Figure 15.

The two-phase zone is approximately at the saturation temperature (boiling temperature) and the length of the two-phase zone increases with time. Moreover, the vapor front propagates upward with time and an excess pore water pressure of about 1.8 kPa is generated in the two-phase zone. Shown in Figure 15, the propagation speed of the simulated centerline vapor front is about 0.49 m/hr and compares well with the experimental vapor front propagation speed of 0.59 m/hr. Here, the centerline vapor front is defined as the lowest location where the liquid saturation $S = 1$ along the centerline. Equivalently, it is the leading edge of the two-phase zone along the centerline. It is noted that the transport behavior in regions with the column

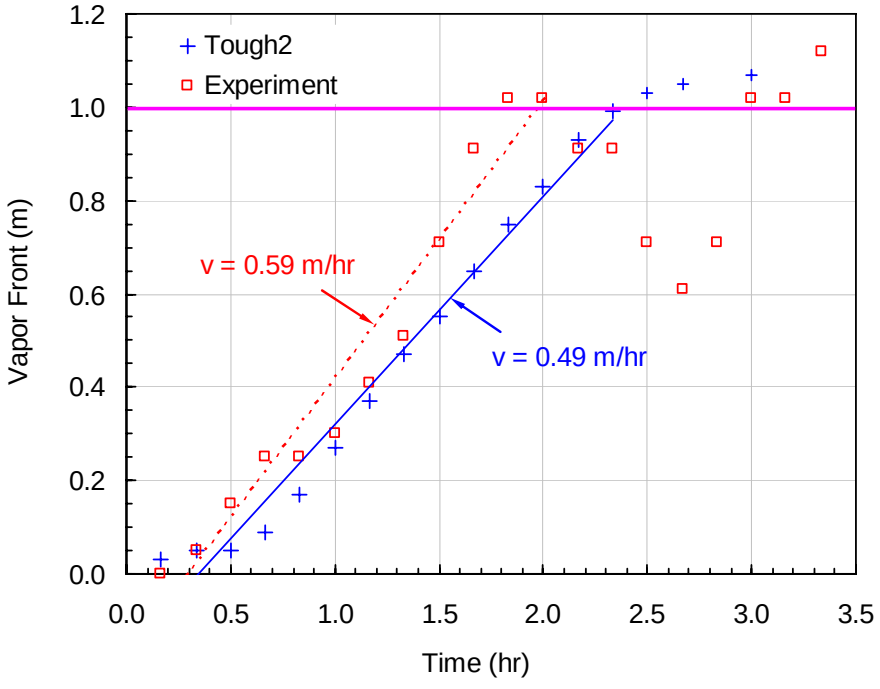

Figure 15. TOUGH2 simulations of the centerline vapor front for the saturated coarse sand soil column experiment ($\dot{q}'' = 30$ kW/m^2)

height $z > 1$ m can be strongly affected by the top water column, so only the column region $z \leq 1$ m is considered in this analysis. Figure 16 shows the excess pore water pressure generated in the soil column. The excess pore water pressure is defined as the difference between the pore water pressure and the hydrostatic pore water pressure which corresponds to the pore water pressure at $t = 0$. It can be seen that the maximum excess pore water pressure at the base of the column is about 1.8 kPa, which is equivalent to 8% of the overburden pressure at the base of the soil column before heating and 18% of the effective stress carried out by the solid matrix at this same location. This value is lower than the excess pore water pressure measured in experiments, which is about 4 kPa, equivalent to 18% of the overburden pressure at the base of the soil column before heating and 40% of the effective stress at the same location.

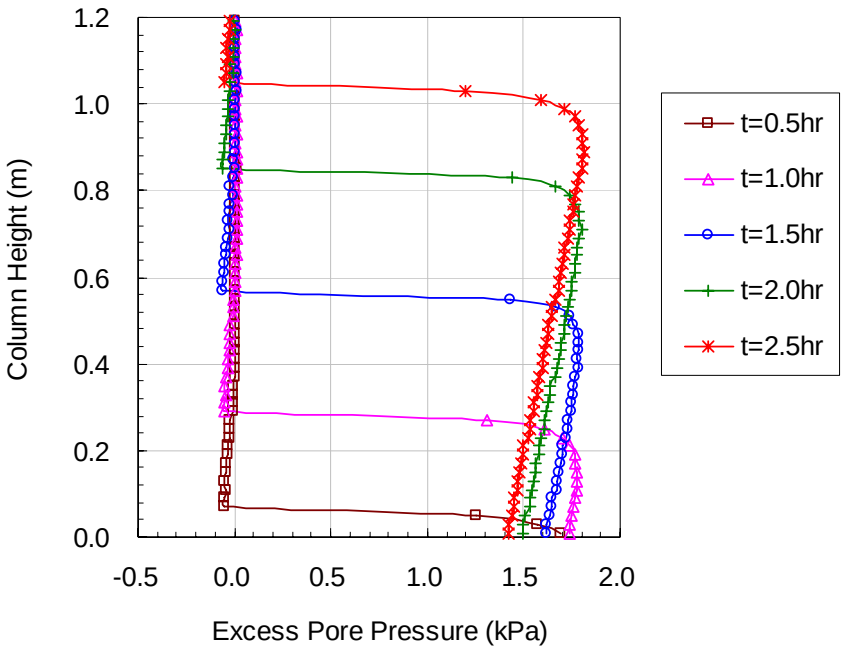

Figure 16. TOUGH2 simulations of excess pore water pressures along the centerline for the saturated coarse sand soil column experiment ($\dot{q}'' = 30$ kW/m^2)

In addition, the two-phase zone has a countercurrent flow of upward vapor and downward liquid from the evaluation of liquid and vapor mass flux profiles (not shown here). This flow pattern is consistent with that described in the literature [4, 6 - 8], but different from that in FLUENT. As described in §3.2, the two-phase zone in FLUENT has upward flow on the sides and downward flow in the middle. It is interesting to note that the degree of liquid saturation still maintains a large value ($0.76 \le S < 1$) in the two-phase zone, indicating it is far from establishing a dry-out vapor region.

The transport behavior in the saturated coarse sand is also sensitive to changes in the net basal heat flux. For a given saturated coarse sand, the penetration depth of the vapor front and the propagation speed of the vapor front increase with the increase of the net basal heat flux. Figure 17 shows the comparison of the vapor fronts when the saturated coarse sand is heated by a net basal heat flux of 11.55 kW/m^2, 30 kW/m^2 and 33 kW/m^2. For a net basal heat flux of 11.55 kW/m^2, the vapor front only can form after 2.5 hours and then it propagates upward with a speed of 0.21 m/hr. But for a net basal heat flux of 30 kW/m^2 and 33 kW/m^2, the vapor front forms before 10 minutes and the front propagates upward with a speed of about 0.49 m/hr and 0.54 m/hr respectively.

Different from the vapor front propagation behavior, for a given soil, the maximum pore water pressure established in the soil column doesn't change significantly with the increase of the net basal heat flux after boiling occurs. Shown in Table 5, when the net basal heat flux changes from 11.55 kW/m^2 to 33 kW/m^2, the maximum excess pore water pressure at the base of the soil column is almost a

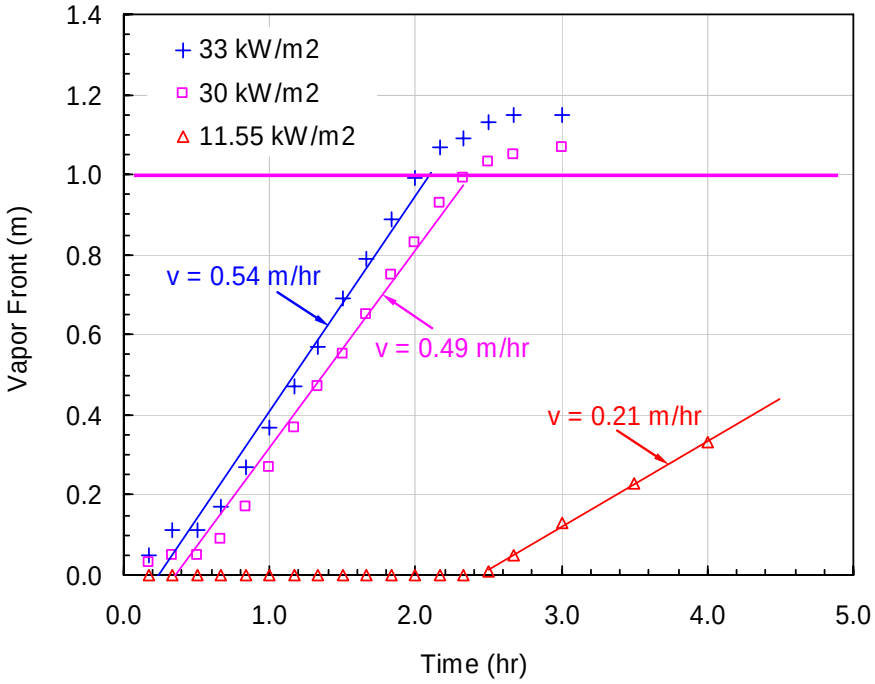

Figure 17. TOUGH2 simulations of the centerline vapor front for the saturated coarse sand soil column under different net basal heat fluxes

constant. This is consistent with Campanella's study [20] in which he determines that the excess pore water pressure in the soil doesn't change when the temperature variation of the soil is the same.

Table 5. Excess pore water pressures under different net basal heat flux

Net basal heat flux	11.55 kw/m^2	30 kW/m^2	33 kW/m^2
Maximum excess pore water pressure	1.5 kPa	1.8 kPa	1.8 kPa

It is also interesting to note that the convection region in the liquid zone is longer when the net basal heat flux decreases and this extension of the convection region due to the growth of the convection cells can overwhelm the formation of the

vapor front during some initial heating period. For example, the length of the convection area in the 33 kW/m^2 case shown in Figure 18 is 0.2 m and is almost a constant before 2 hours. But in the 11.55 kW/m^2 case shown in Figure 19, the length of the convection region becomes longer with time before the vapor front forms at $t = 2.5$ hours, because of the convection cell growth. After that, the length of the convection region almost maintains a constant of about 0.8 m and the vapor front propagates upward. It can be inferred from Figure 19 that the extension of the convection region due to the convection cell growth overwhelms the formation of the vapor front before 2.5 hours.

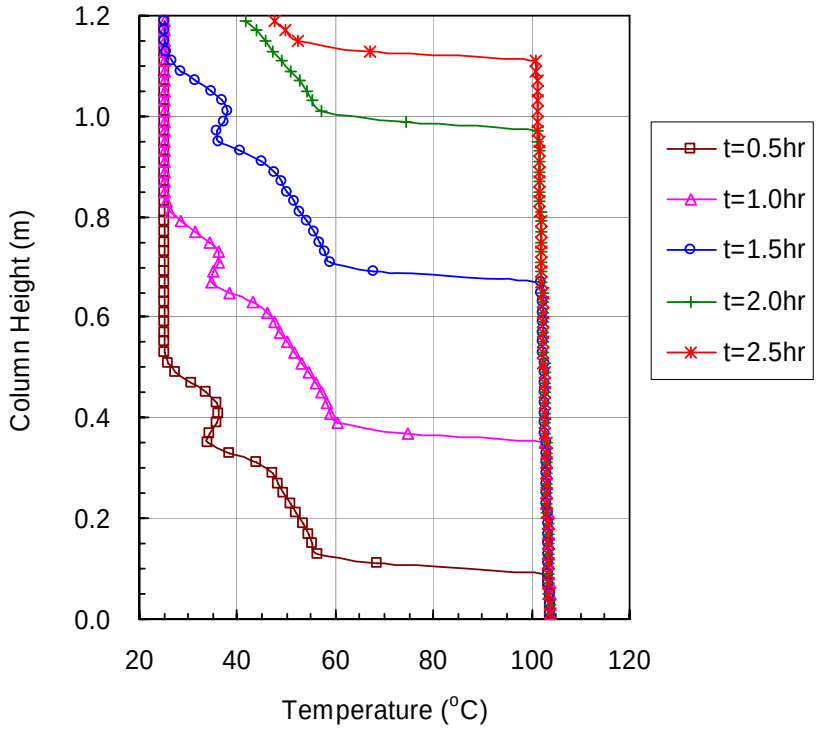

Figure 18. TOUGH2 simulations of centerline temperatures for the saturated coarse sand soil column ($\dot{q}'' = 33$ kW/m^2)

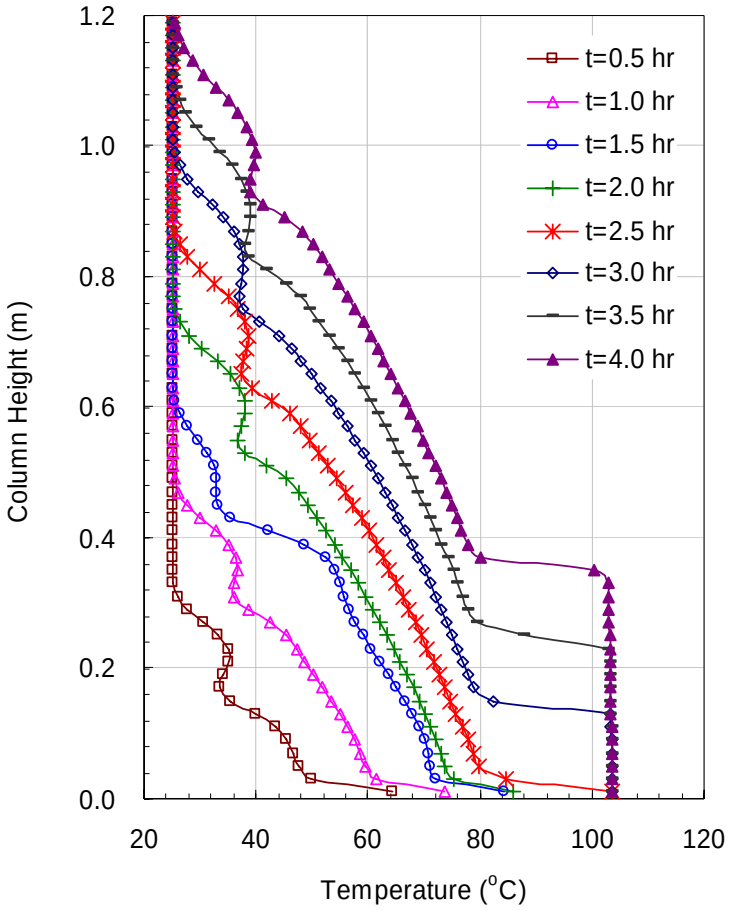

Figure 19. TOUGH2 simulations of centerline temperatures for the saturated coarse sand soil column ($\dot{q}'' = 11.55$ kW/m^2)

3.3.2 Saturated fine sand

Compared with the transport behavior of the saturated coarse sand described above, the saturated fine sand has some different responses to intense heating due to relatively smaller porosity and permeability. These differences include the suppression of natural convection in the liquid zone and higher excess pore water pressures generated in the soil.

Similar to the saturated coarse sand case, reasonable agreement is achieved between TOUGH2 simulations and the reference experiment case [3]. Shown in

Figure 20, simulation results agree well with the experimental measurements when $t \leq 2.5$ hours. But after 2.5 hours, the simulated saturation temperature front is much higher than that in experiments because the experimental vapor front propagates intermittently, as shown in Figure 21 and described later in this section.

A two-zone structure is also formed in the saturated fine sand soil column, namely a liquid zone on the top and an underlying two-phase zone at the bottom. In the liquid zone, no natural convection cell forms and also no 'S-shaped' curve is observed in the centerline temperature profiles shown in Figure 20. The two-phase zone is approximately at the saturation temperature and has a countercurrent flow of

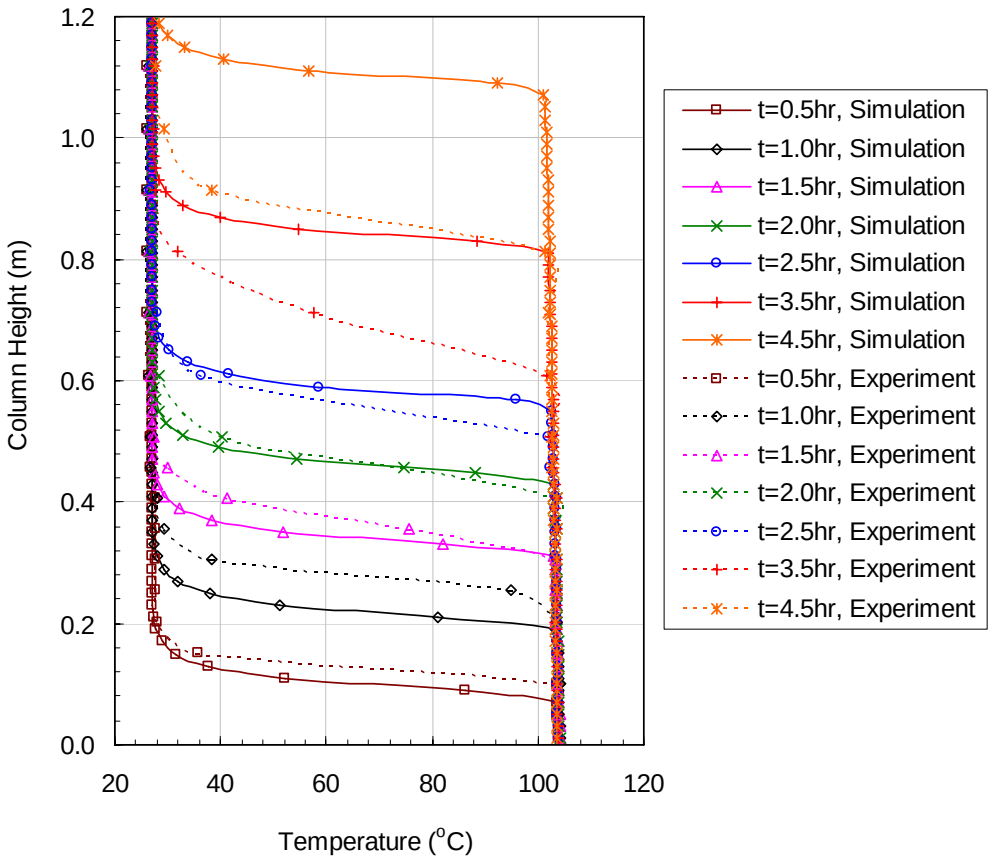

Figure 20. TOUGH2 simulations of centerline temperatures for the saturated fine sand soil column experiment ($\dot{q}'' = 11.55$ kW/m^2)

upward vapor and downward liquid. The length of the two-phase zone increases with time. Moreover, the vapor front propagates upward with a constant speed and an excess pore water pressure of about 3.5 kPa is generated in the two-phase zone. Additionally, the degree of liquid saturation in the two-phase zone is $0.45 \le S < 1$, which is a little smaller than that in the saturated coarse sand but is still far from establishing a dry-out vapor zone.

TOUGH2 simulations give a linear centerline vapor front with a propagation speed of about 0.25 m/hr, but experimental measurements show an intermittently advancing centerline vapor front with a propagation speed of about 0.20 - 0.21 m/hr for each step. As shown in Figure 21, the vapor front and its propagation speed in simulations agree well with those in experiments before 2.5 hours. After 2.5 hours, the experimental data show some steps of the centerline vapor front but the propagation speed of each step is similar with each other and also approximate to the simulated propagation speed. It is unclear why the experimental data show an intermittently advancing centerline vapor front. Possibly it is related to the transition between conduction and convection in the liquid zone or the transition of the convection modes if natural convection happens. Another possibility is that migration of the soil particles happens at some local points at that time due to the decrease of the effective stress carried out by the solid matrix. When soil particles migrate, some local points will have higher permeability and contain more water so that the vapor front propagation can be suppressed at some initial time. In §3.3.3, it will be proven that the vapor front of the saturated fine sand will move upward faster than that of the

saturated coarse sand at the first 2.5 hours when they are subjected to the same net basal heat flux of 11.55 kW/m^2.

The excess pore water pressure generated in the saturated fine sand soil column is much higher than that in the coarse sand soil column. As shown in Figure 22, the maximum excess pore water pressure at the base of the saturated fine sand soil column is about 3.5 kPa, which is equivalent to 14% of the overburden pressure at the base of the soil column before heating and 29% of the effective stress carried out by the solid matrix at the base before heating. The simulated excess pore water pressure is lower than that measured in experiments, which is about 6.5 kPa, equivalent to 26% of the overburden pressure at the base before heating and 54% of the effective stress at the same location.

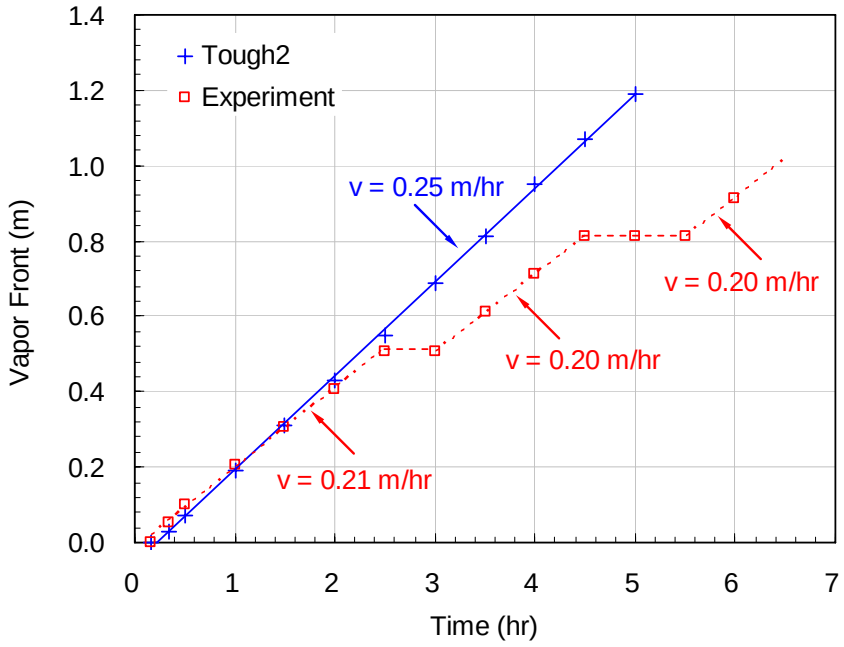

Figure 21. TOUGH2 simulations of centerline vapor front for the saturated fine sand soil column experiment ($\dot{q}'' = 11.55$ kW/m^2)

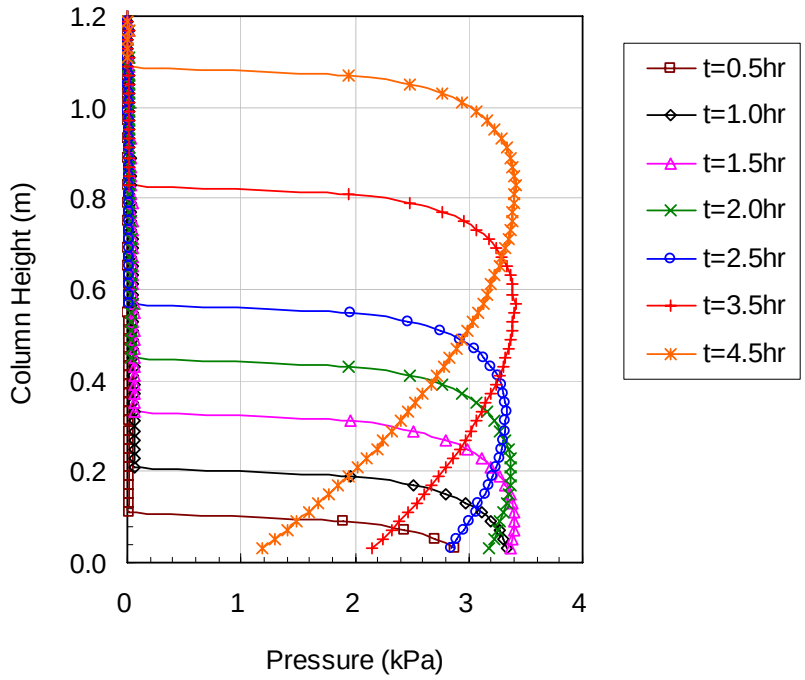

Figure 22. TOUGH2 simulations of excess pore water pressures along the centerline for the saturated fine sand soil column experiment ($\dot{q}'' = 11.55$ kW/m^2)

3.3.3 Comparison of the coarse sand response and the fine sand response

From above analyses, it can be seen that the maximum excess pore water pressure established in the saturated coarse sand is much lower than that generated in the saturated fine sand at same time. For similar incident heat flux (e.g., the total radiant heat given off by the heater or the total radiant heat from a tunnel fire), the vapor front propagation in the saturated coarse sand is faster than that in the saturated fine sand.

However, this conclusion of the vapor front propagation is not valid when the saturated coarse sand and the saturated fine sand subject to the same net basal heat flux. Figure 23 shows comparisons of the centerline vapor front propagation between

the saturated coarse sand and the saturated fine sand when they are heated by a same net basal heat flux of 11.55 kW/m^2. For the saturated coarse sand, it takes 2.5 hours to form the centerline vapor front. Before 2.5 hours, the growth of convection cells in the liquid zone suppresses the formation of the centerline vapor front as discussed in §3.2.1. But for the saturated fine sand, it only takes less than 10 minutes to generate the vapor front because no convection cell happens in the liquid zone in the saturated fine sand. Therefore, the centerline vapor front penetrates deeper in the saturated fine sand than that in the saturated coarse sand before 2.5 hours. However, after the vapor front also forms in the saturated coarse sand (after 2.5 hours), they have similar front propagation speeds which are 0.25 m/hr for the saturated fine sand and 0.21 m/hr for the saturated coarse sand.

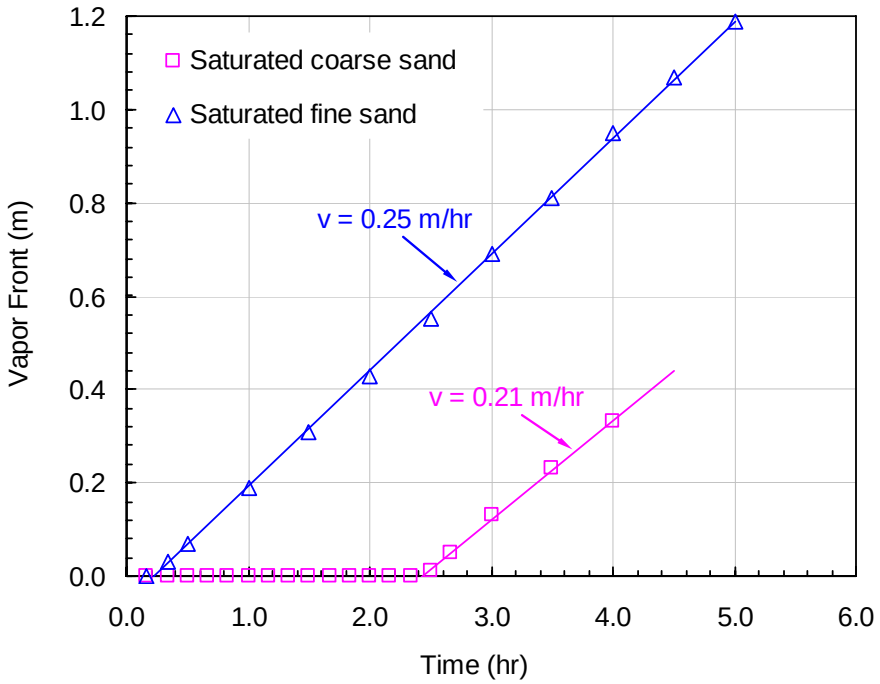

Figure 23. Comparison of the centerline vapor front propagation between saturated coarse sand and saturated fine sand ($\dot{q}'' = 11.55$ kW/m^2)

To summarize, the saturated fine sand can generate a larger excess pore water pressure than the saturated coarse sand. But the speed and associated penetration depth of the vapor front depend on the net basal heat flux. When the saturated coarse sand and the saturated fine sand are heated by a similar incident heat flux, the saturated coarse sand exhibits a faster propagation speed and a deeper penetration depth of the vapor front. When they are heated with the same net basal heat flux, the saturated fine sand has an earlier propagation of the vapor front, because the growth of convection cells suppresses the vapor front in the saturated coarse sand.

Chapter 4: Summary and Conclusions

This study investigates the response of saturated soils to intense heating from tunnel fires by numerical simulation. The complete set of conservation equations for porous media in commercial CFD software and the reduced set of conservation equations commonly used for porous media are reviewed. Two-dimensional numerical models are established and 2-D simulations are conducted using FLUENT and TOUGH2.

The main results from this study are summarized as below:

1) The treatment for porous media in FLUENT is basically to add a momentum sink into the general flow equation. To include the boiling phenomena into FLUENT, a boiling and condensation model is required.
2) The governing equations in TOUGH2 are the same as the common equations presented in porous media literatures. Steam table equations are used to calculate the water properties and describe the boiling and condensation phenomena.
3) Models for capillary effects and relative permeability are required to describe the experimentally observed transport behavior. Without considering them, FLUENT gives an inconsistent dry-out vapor zone at the base of the soil column. TOUGH2 which includes these models gives the same two-zone structure observed in experiments, namely a liquid zone on the top and a two-phase zone at the bottom.

4) Reasonably qualitative agreement is achieved between 2-D TOUGH2 results and experimental data, regarding centerline temperature profiles, the vapor front propagation and the maximum excess pore water pressure. For the saturated coarse sand under $\dot{q}'' = 30\,\mathrm{kW/m^2}$, the propagation speed of the vapor front and the maximum excess pore water pressure are 0.49 m/hr and 1.8 kPa in TOUGH2, while 0.59 m/hr and 4 kPa in experiments. For the saturated fine sand under $\dot{q}'' = 11.55\,\mathrm{kW/m^2}$, they are 0.25 m/hr and 3.5 kPa in TOUGH2, while 0.20 m/hr and 6.5 kPa in experiments.

5) The vapor front propagation of the saturated coarse sand is sensitive to the basal heat flux. With increases in the net basal heat flux, the penetration depth of the vapor front and the propagation speed of the vapor front increase. At low basal heat fluxes, the extension of the convection region due to the growth of convection cells in the liquid zone can suppress the formation of the vapor front during some initial heating period. However, the maximum excess pore water pressure is approximately the same under different heat fluxes.

6) The saturated fine sand can generate a higher excess pore water pressure inside the soil column than the saturated coarse sand. However, the penetration depth and speed of the vapor front depend on the heat flux. When they are heated by a similar incident heat flux (e.g., the heat flux given off from the lab radiant heater or a tunnel fire), the saturated coarse sand exhibits a faster propagation speed and a deeper penetration depth of the vapor front. When subjected to the same net basal heat flux in this study,

the saturated fine sand has an earlier propagation of the vapor front, but the propagation speed of the vapor front is similar after the vapor front also forms in the saturated coarse sand.

Although the 2-D modeling can greatly save simulation time and these 2-D simulation results in TOUGH2 are encouraging, they are not yet sufficient to rigorously verify the model, since 2-D simulations may not represent the convention details in a 3-D geometry. More work is suggested in the future including:

1) 3-D cylinder simulations for saturated soils to compare differences between 2-D simulations, 3-D simulations and reference experiments. These comparisons should be able to determine whether the 2-D simulation is enough to model this problem, regarding the results we need such as the excess pore water pressure and the vapor front propagation speed;
2) Large scale tunnel simulations using the verified numerical model and combined with the tunnel fire model.

Appendices

Appendix A. Modeling Natural Convection Problems in FLUENT

Porous media are modeled by adding a momentum sink into the standard fluid flow equation in FLUENT, so that the momentum equation solved in FLUENT is a little different from the Darcy momentum equations used commonly for porous media. To verify the suitability of using FLUENT to model porous media, a 3-D natural convection problem without boiling is modeled at first and the results are verified with Bau's experimental results [4].

Figure 24 shows the comparison of centerline temperatures between the numerical results and Bau's theoretical and experimental results. The parameters used are T_∞ = 300 K, T_b = 365 K, H = 0.2 m, D = 0.095 m, φ = 0.42, K = 1.374E-9 m^2, λ = 2.15 W/m-K. The numerical results are approximate to the experimental results, so it is basically suitable to use FLUENT to model the porous medium problem.

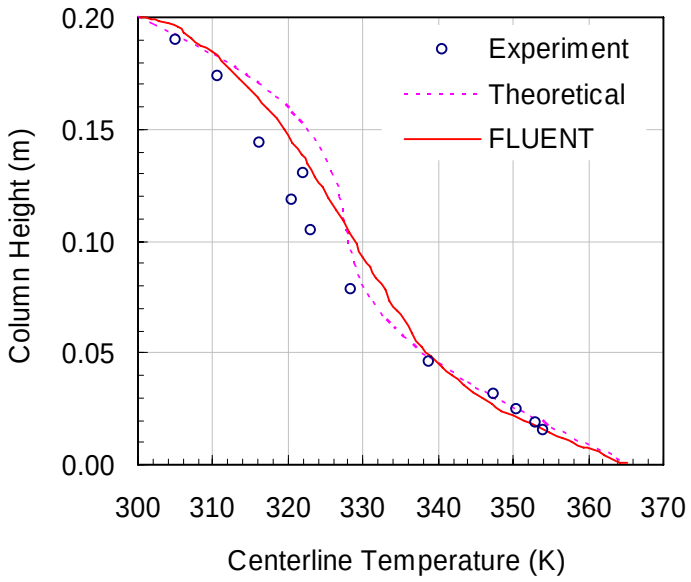

Figure 24. Comparison of centerline temperatures without boiling in FLUENT

Bibliography

1. http://home.no.net/lotsberg/link_7.html#Tunnel%20Safety
2. Lonnermark, A., *On the characteristics of fires in tunnels*, Ph.D. thesis, Lund University, Sweden, 2005.
3. Yong, M. W., *Extreme geotechnical response to high heat from tunnel fires*, M.S. thesis, University of Maryland at College Park, 2004.
4. Bau, H.H., *Experimental and theoretical studies of natural convection in laboratory-scale models of geothermal systems*, Ph.D. thesis, Cornell University, Ithaca, NY, 1980.
5. Bau, H. H. and Torrance, K. E., Low Rayleigh number thermal convection in a vertical cylinder filled with porous materials and heated from below, *Transaction of the ASME, Journal of Heat Transfer*, Vol. 106, 1982, pp. 166-172.
6. Bau, H.H., Torrance, K.E., Boiling in low-permeability porous materials, *International Journal of Heat Mass Transfer*, Vol. 25, No. 1, 1982, pp. 45-55.
7. Udell, K.S., Heat transfer in porous media heated from above with evaporation, condensation and capillary effects, *Journal of Heat and Mass Transfer*, Vol. 105, 1983, pp. 485-492.
8. Udell, K.S., Heat transfer in porous media considering phase change and capillarity-the heat pipe effect, *Int. J. Heat Mass Transfer*, Vol. 28, No.2, 1985, pp. 485-495.
9. Faust, C.R. and Mercer, J.W., Geothermal reservoir simulation 1. Mathematical models for liquid- and vapor- dominated hydrothermal systems, *Water resources research*, Vol. 15, No.1, 1979, pp.23-30.

10. Roberts, P.J. and Lewis, R.W., An extension of the thermodynamic domain of a geothermal reservoir simulator, *Transport in Porous Media*, Vol.2, 1987, pp. 397-420.
11. Ramesh, P.S. and Torrance, K.E., Numerical algorithm for problems involving boiling and natural convection in porous materials, *Numerical Heat Transfer*, Part B, Vol. 17, 1990, pp.1-24.
12. Wang, C.Y., Beckermann C. and Fan C., Numerical study of boiling and natural convection in capillary porous media using the two-phase mixture model, *Numerical Heat Transfer*, Part A, Vol. 26, 1994, pp. 375-398.
13. Wang, C.Y. and Beckermann C., A two-phase mixture model of liquid-gas flow and heat transfer in capillary porous media - I. Formulation, *International Journal of Heat Mass Transfer*, Vol, 36, No. 11, 1993, pp. 2747-2758.
14. Wang, C.Y. and Cheng, P., A multiphase mixture model for multiphase, multicomponent transport in capillary porous media - I. Model development, *International Journal of Heat Mass Transfer*, Vol, 39, No. 17, 1996, pp. 3607-3618.
15. Shi, B., *Boiling heat transfer in porous media with/without chimneys*, Ph.D. thesis, University of Illinois at Urbana-Champaign, 1994.
16. Shi, B., Numerical modeling of boiling heat transfer in porous media, HTD-Vol. 331, *National Heat Transfer Conference*, Vol. 9, ASME 1996, pp. 15-24.
17. Benard, J., Eymard R., etc., Boiling in porous media: model and simulations, *Transport in Porous Media*, Vol.60, 2005, pp. 1-31.

18. Daurelle, J.V., Topin F. and Occelli, R., Modeling of coupled heat and mass transfers with phase change in a porous medium: application to superheated steam drying, *Numerical Heat Transfer*, Part A, Vol. 33, 1998, pp. 39-63.
19. Ollivella, S. and Gens, A., Vapor transport in low permeability unsaturated soils with capillary effects, *Transport in Porous Media*, Vol. 40, 2000, pp.219-241.
20. Campanella, R. G. and Mitchell, J. K., Influence of temperature variations on soil behavior, Journal of Soil Mechanics and Foundations Division, *Proceedings of the American Society of Civil Engineers*, SM3, 1968, pp.709-733.
21. Rutqvist, J., Wu, Y. S., etc., A modeling approach for analysis of coupled multiphase fluid flow, heat transfer, and deformation in fractured porous rock, *International Journal of Rock Mechanics & Mining Science*, Vol. 39, 2002, pp. 429-442.
22. Gens, A., Garcia-molina, A. J., etc., Analysis of a full scale in situ test simulating repository conditions, *International Journal for Numerical and Analytical Methods in Geomechanics*, Vol. 22, 1998, pp. 515-548.
23. Rutqvist, J., Barr, D., etc., Coupled thermal-hydrological-mechanical analyses of the Yucca Mountain Drift Scale Test – Comparison of field measurements to predictions of four different numerical models, *International Journal of Rock Mechanics & Mining Sciences*, Vol. 42, 2005, pp. 680-697.
24. FLUENT6.2 Userguide.
25. CODE_BRIGHT Userguide.
26. TOUGH2 Userguide.
27. Petrasim Userguide.

28. Nield, D.A. and Bejan A., *Convection in porous media*, second edition, Springer-Verlag New York, Inc., 1999.

29. Collier, J.G., *Convective boiling and condensation*, 2nd Edition, McGraw-Hill Co., New York, NY, 1980.

30. Fredlund, D. G. and Rahardjo, H., *Soil mechanics for unsaturated boils*, John Wiley & Sons, Inc., 1993.

31. http://www.omega.com/literature/transactions/volume1/emissivityb.html.